学 位 論 文（要約）

Construction of Catalytic Reaction Nano-spaces in a Porous Molecular Crystal, Metal–Macrocycle Framework (MMF)

(多孔性分子結晶 Metal–Macrocycle Framework (MMF)のナノ空間を用いた触媒反応場の構築)

平成 29 年 12 月博士（理学）申請

東京大学大学院理学系研究科
化学専攻

米澤　拓孝

Abstract

1. Introduction

Nano-spaces around active sites of enzymes play important roles in controlling reactions (Figure 1a). Inspired by the molecular behaviors, a variety of reaction nano-spaces with catalytic active sites have been constructed in coordination cages and porous materials which provide high specificity, efficiency, and selectivity of the reactions. However, it is still challenging to design functional nano-spaces based on multi-point and site-selective interactions between substrates and inner surfaces in such a confined space.

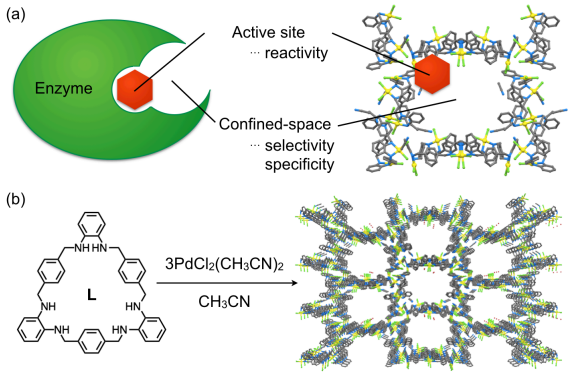

Figure 1. (a) Schematic views of active sites in a confined-space of enzyme and metal–macrocycle framework (MMF). (b) Synthesis of MMF.

A porous molecular crystal, metal–macrocycle framework (MMF), can be constructed from a macrocyclic hexaamine **L** and $PdCl_2$ (Figure 1b). MMF has one-dimensional nano-channels with a 1.4 × 1.9 nm^2 dimension, and five enantio-paired molecular binding sites are arranged on the inner surfaces. Such confined spaces with inner surfaces in MMF have high potential as catalytic reaction nano-spaces which allow highly specific, efficient, and selective reactions based on the multi-molecular adsorption with high site-selectivity.

In this study, I have constructed reaction nano-spaces with catalytic active sites in MMF for the development of space-specific reactions. Specifically, non-covalent immobilization of *p*-toluenesulfonic acid (*p*-TsOH) in MMF was conducted for a size-specific acid-catalyzed reaction. Moreover, it was found that photo-activation of the Pd centers on the surfaces of MMF channels provides an excellent platform for olefin migration reactions.

2. Non-covalent immobilization of an acid catalyst in MMF for a size-specific reaction

In my master course study, in the light of the fact that a variety of substituted benzene molecules site-selectively bind to macrocyclic cavity-derived pockets, I found that *p*-TsOH immobilized in MMF can catalyze a size-specific deprotection reaction in a preliminary experiment. Then, in my doctoral course study, I optimized the reaction condition and quantitatively analyzed the reaction to examine the effects of the channel structure of MMF with a given dimension on the catalytic reactivity and the reusability of MMF as a heterogeneous catalyst.

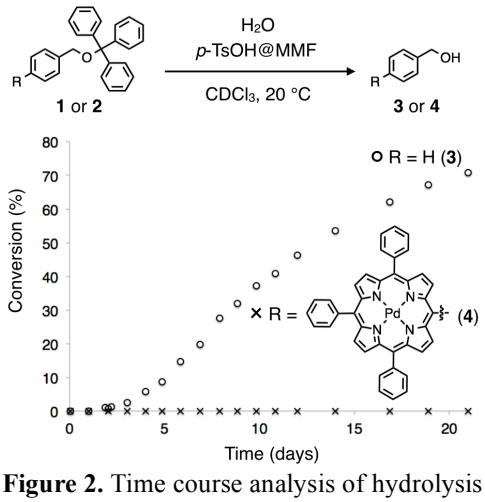

Figure 2. Time course analysis of hydrolysis reaction with 6 mol% of *p*-TsOH@MMF.

The acid-catalyst, *p*-TsOH@MMF, which includes approximately 1.6 *p*-TsOH molecules per a unit-space, was prepared by soaking MMF crystals in a solution of *p*-TsOH·H_2O in acetonitrile and successive washing with dichloromethane to remove excess *p*-TsOH from the channel spaces. There was a concern that the immobilized *p*-TsOH would be dissociated from the inner surface of MMF due to the non-covalent binding. However, the catalyst was stably adsorbed to the surface during the reaction under this condition and was therefore reusable. The deprotection reactions of the trityl-protected $PhCH_2OCPh_3$ **1** and Pd-$TPPCH_2OCPh_3$ **2** (Pd-TPP = palladium tetraphenylporphyrinato) were compared in the presence of a catalytic amount of *p*-TsOH@MMF possessing channels with a 1.4 × 1.9 nm^2 dimension. The reaction proceeded with the smaller **1** in up to 70% yield, whereas no reactions were observed with the larger **2** even after three weeks (Figure 2). This result indicates that only the substrate incorporated in the channel can be catalyzed in a highly size-specific manner.

3. Development of photo-induced olefin migration in MMF

Stable coordination bonds often become more labile by external stimuli such as light, and generate reactive species. In this study, the Pd centers exposed to the inner space of MMF were successfully activated by light to catalyze olefin migration (Figure 3). The mechanism of this reaction was then examined both experimentally and theoretically.

The inclusion of 4-allyl anisole **5** in MMF was confirmed by single-crystal X-ray diffraction and NMR measurements after soaking in a solution of **5** in acetonitrile. MMF crystals including **5** yielded an olefin-migrated product **6** quantitatively under photo-irradiation, whereas no reactions took place in the dark (Scheme 1). Moreover, even photo-irradiation around 450 nm, though more slowly, promoted the reaction. This suggests that the olefin migration be promoted by a photo-activated species generated in MMF.

Deuterated 4-allyl anisole (**5**-*DD*) was used to clarify the reaction mechanism. A 1,2-D shift product **6**-*DDH* and the less deuterated product **6**-*DHH* were detected in addition to a 1,3-D shift product **6**-*DHD* (Figure 4). This result suggests that the olefin migration was catalyzed by Pd-H species *via* a well-known alkyl mechanism involving intermolecular

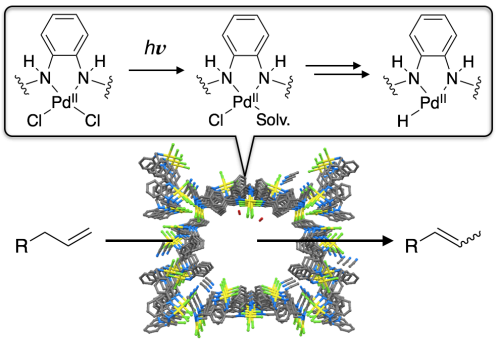

Figure 3. Schematic representation of olefin migration reaction with photo-activated Pd species.

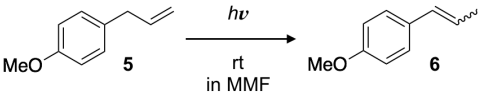

Entry	Light source (nm)	Time (h)	Yield (%)
1	280 ~ 630	2	91
2	450 ± 10	12	8
3	no irradiation	12	0

Scheme 1. Wavelength dependence of photo-induced olefin migration. The *E*/*Z* ratio was over 10.

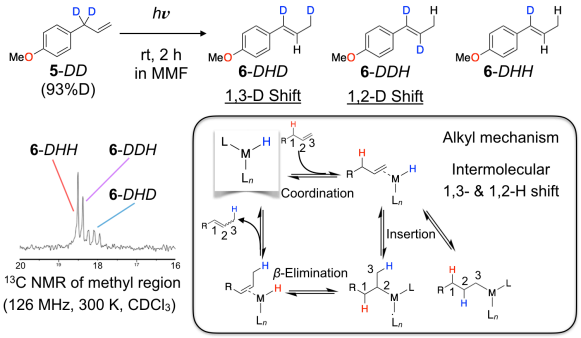

Figure 4. Deuterium labelling experiment. The inset shows a generally proposed alkyl mechanism.

1,3- and 1,2-H shift mechanisms.

Photo-activation of the Pd centers in MMF was assessed by MS-CASPT2 calculation using a model complex, a $PdCl_2$ complex of *N*,*N*′-diethyl-*o*-phenylenediamine. The vertical excitation spectrum suggests the strong absorption bands around 295 and 457 nm attributable to electron transitions toward σ^* orbital of the Pd-Cl bond. This orbital was possibly assigned to an antibonding orbital of the Pd-Cl bond, suggesting photo-cleavage by light absorption in the absorption regions. In addition, single-crystal XRD analysis before and after two-hour photo-irradiation at –180 °C was conducted for the direct observation of the Pd-Cl bond cleavage by photo-irradiation. In comparison of the electron density maps, the significant decrease in the electron density around Cl9 indicates the site-selective photo-cleavage of the Pd5-Cl9 bond (Figure 5).

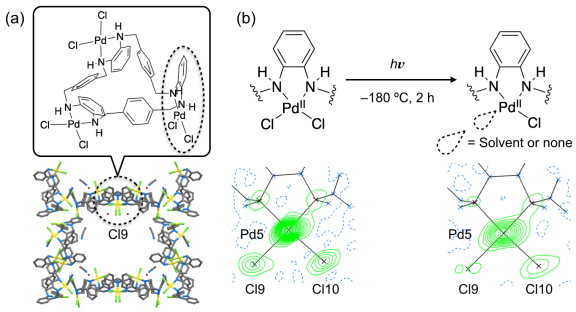

Figure 5. (a) Enlarged partial structure of MMF. (b) Direct observation of the Pd-Cl cleavage under photo-irradiation.

Taken all together, the photo-cleavage of the Pd-Cl bond of Pd centers in MMF appears to occur in a site-selective manner leading to successive formation of reactive Pd-H species, which would promote the Pd-catalyzed olefin migration *via* the alkyl mechanism.

4. A preferential photoreaction in a confined MMF nano-space

Photo-reactive substrates were expected to show a different reactivity in a confined MMF nano-space. Then, 1,6-dienes **7a** and **7b**, which normally provide an intramolecular [2+2] cycloadduct under photo-irradiation, was examined in MMF (Figure 6). 1,6-Diene **7a** in MMF was converted into an internal olefin **9a** in 20% yield under photo-irradiation, whereas **7a** in acetonitrile was converted into a [2+2] cycloadduct **8a** in 87% yield under photo-irradiation and no olefin migration reactions took place at all. For reference, **7b** in MMF resulted in no reactions due to the presence of two methyl groups on the allylic position, whereas [2+2] cycloaddition proceeded in acetonitrile. This result indicates that the [2+2] cycloaddition of **7a** in MMF was completely inhibited and the reaction proceeded through a different pathway to form an olefin migration product.

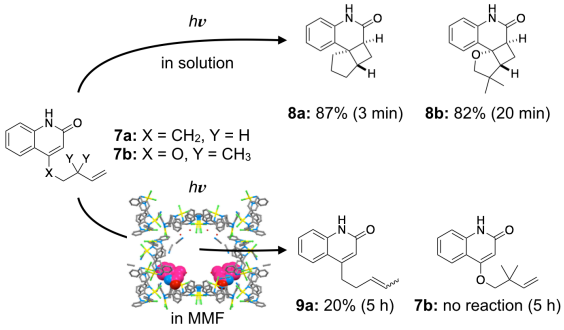

Figure 6. Comparison of the reactivity of 1,6-dienes, **7a** and **7b**, in solution and MMF.

A photo-shielding effect of MMF was then considered as a cause of inhibition. However, *cis*/*trans* photo-isomerization of azobenzene proceeded in MMF, though slowly. From a viewpoint of solvation in a confined space, a suitable conformation is required to facilitate the intramolecular [2+2] cycloaddition. As found in the model experiments, [2+2] cycloaddition was strongly suppressed in a frozen solvent (CD_3CN, –78 °C) and molecular crystals of **7a**, whereas the reaction proceeded in cooled solvents (CD_3OD and toluene-d_8, –78 °C) (Scheme 2). This result suggests that the mobility of molecules have a large effect on the [2+2] cycloaddition of **7a**. Single-crystal XRD and NMR analyses suggest that **7a** in MMF adsorbed with a high occupancy to one of the binding sites through two hydrogen bonds (Figure 7). Therefore, the inhibition of [2+2] cycloaddition can be well explained by the unfavorable binding conformation of **7a**, its restricted conformation due to the lower mobility of solvating molecules, and, though to a lesser extent, the photo-shielding effect of MMF.

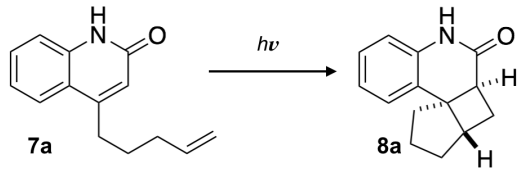

Entry	Conditions	Time (min)	Conversion (**7a**, **8a**, %)
1	in CD_3CN, rt	3	0%, 87%
2	in CD_3CN, -78 °C	120	87%, 9%
3	in molecular crystal, rt[a]	120	98%, 2%
4	in CD_3OD, -78 °C	10	0%, 91%
5	in toluene-d_8, -78 °C	10	0%, 92%

Scheme 2. [2+2] cycloaddition of **7a** in various reaction media.

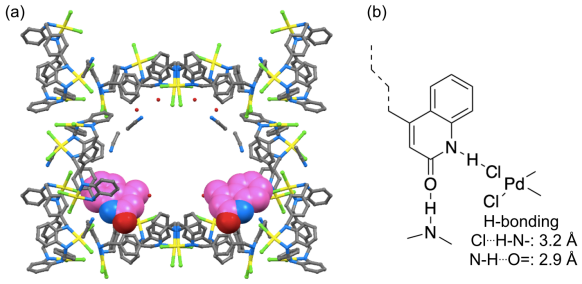

Figure 7. (a) Binding mode of **7a** to the inner surface of MMF. (b) Hydrogen-bonded interactions between **7a** and the Pd-center.

5. Conclusion

In my doctoral course study, I have established efficient ways to construct catalytic reaction nano-spaces by introducing active sites into confined MMF nano-spaces. A size-specific reaction depending on the channel dimension has been achieved by non-covalent immobilization of an acid catalyst to the inner surface of MMF. Moreover, a Pd-catalyzed olefin migration reaction was realized by the photo-activated Pd centers in MMF forming reactive Pd-H species. Here, the spatial effects of MMF nano-spaces on the chemical reactions were discussed from the viewpoints of the molecular mobility as well as the photo-shielding effect of MMF. Such nano-spaces based on the self-assembly of functional macrocycles would lead to more precisely designed catalytic reaction centers with a different chemical reactivity from those in bulk solvents.

Abbreviations

ATR	attenuated total reflection
a. u.	arbitrary unit
CD	cyclodextrin
DFT	density functional theory
DMF	*N*,*N*-dimethylformamide
DMSO	dimethyl sulfoxide
DRUV	diffuse reflectance ultraviolet-visible
ESI	electrospray ionization
GPC	gel permeation chromatography
H	hydride, hydrogen atom
HRMS	high resolution mass spectroscopy
Hz	hertz
IR	infrared
J	coupling constant
M	molar (mol / L)
MAS	magic-angle-spinning
MOFs	metal–organic frameworks
M.p.	melting point
MS-CASPT2	multi-state complete-active-space second order perturbation theory
m/*z*	mass-to-charge ratio
NMR	nuclear magnetic resonance
ORTEP	Oak Ridge thermal-ellipsoid plot
THF	tetrahydrofuran
TMS	tetramethylsilane
TOF	time of flight
UV-Vis	ultraviolet-visible
XRD	X-ray diffraction
XPS	X-ray photoelectron spectroscopy

Contents

Chapter 1

General introduction

1-1. Strategy of enzymes: active sites in confined spaces

One of the ultimate goals of synthetic chemistry is the development of reactions with high and quantitative efficiency and perfect selectivity. To realize such ideal reactions, various approaches have been examined by developing new catalysts and unveiling the mechanism of reactions experimentally and theoretically. Taking into account of the examples in nature, enzymes in biological system have great ability to control reactions with high efficiency, selectivity, and specificity,[1] which all scientists hope to realize.

The reactions with perfect specificity catalyzed by enzymes are often compared to "lock-and-key". As if a lock could be opened only with a corresponding key, only the limited substrates could be catalyzed by the enzymes. One of the most important factors of this principle is the confined spaces around functional active sites (Figure 1-1).

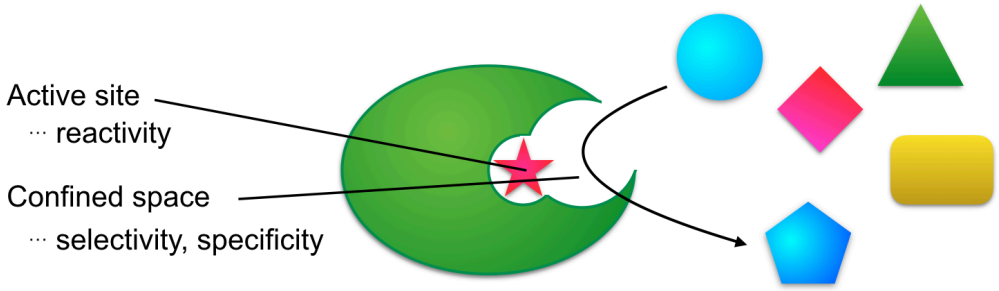

Figure 1-1. Schematic image of an enzyme-catalyzed reaction regulated by the confined space around the active site.

For instance, the thermolysin family is one of the metallopeptidases to hydrolyze a peptide bond.[2] The structures and functions have been well-studied and revealed that the Zn center works as the active site (Figure 1-2). In these analogs, thermolysin and vimelysin have common structural features such as a four-coordinate Zn center with two histidines, one aspartic acid, and one water, and they also show similar catalytic activities to hydrolyze peptides. However, their substrate specificity is different from each other. The peptides with a Leu-Gly-Glu sequence is cleaved by vimelysin but not cleaved by thermolysin. On the other hand, the peptide with a Leu-Gly-Lys sequence is cleaved by thermolysin but not cleaved by vimelysin. This difference in the reaction specificity is derived from the difference in the three-dimensional structures of their confined spaces around the active sites.

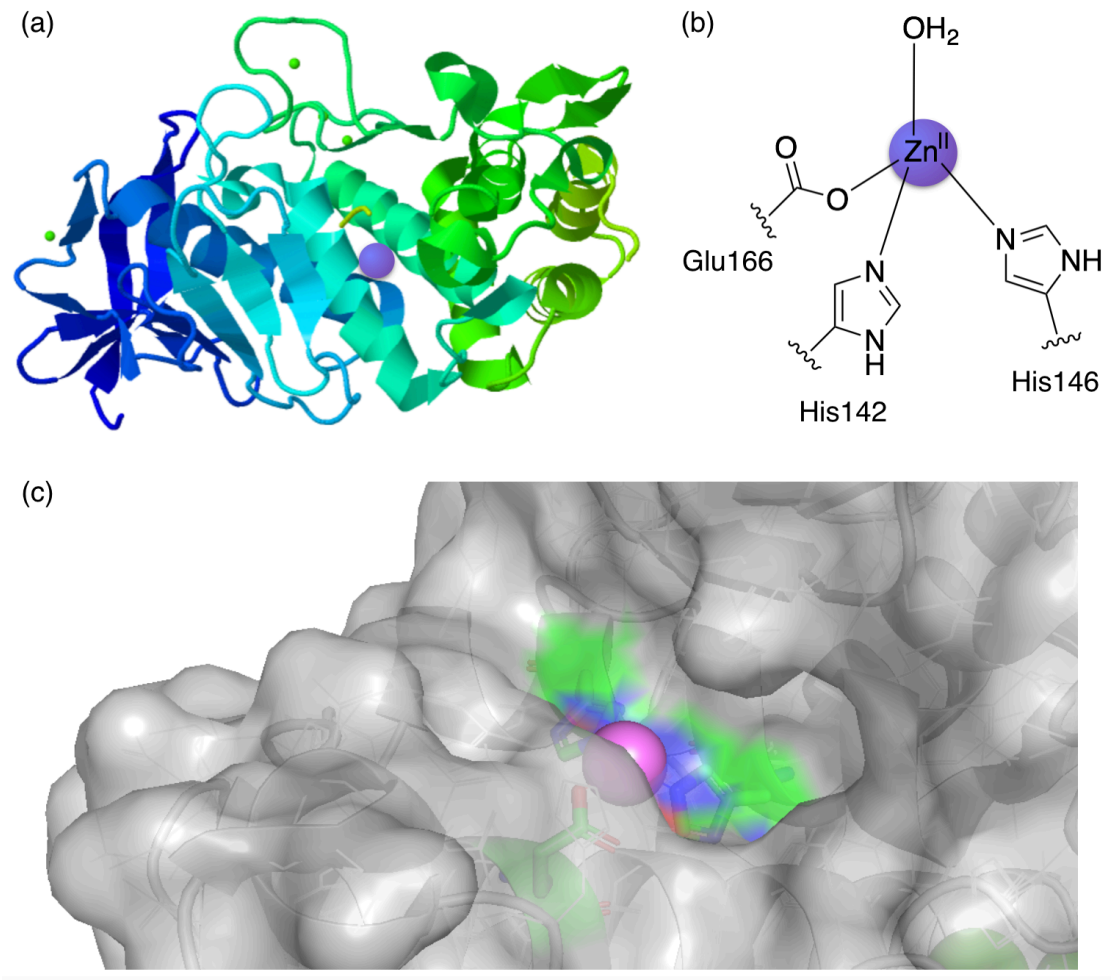

Figure 1-2. (a) Crystal structure of thermolysin (PDB 1KEI). (b) Structure of the Zn active site of thermolysin. (c) Solvent exclusive pore surface of thermolysin around the Zn active site.

As seen in thermolysin and vimelysin, enzymes realize a wide variety of well-regulated reactions owing to the confined nano-spaces as well as the active sites. This strategy, combination of the active sites and the surrounding confined spaces, has strongly inspired chemists to create a new type of catalysts, currently called supramolecular catalysts, toward enzyme-mimic catalysts.

1-2. Artificial catalytic systems inspired by enzymes

Taking into account of the strategy of enzymes, supramolecular catalysts including active sites in confined spaces have been studied to realize highly controlled reactions like enzyme.[3] The first and simple examples of enzyme mimics are chemically-modified cyclodextrins with catalytically active functionalities.[4] The cyclodextrin framework has a well-defined cavity and thereby can recognize reaction substrates with high space-specificity to regulate the reactions. For example, the regio-selective hydrolysis reaction of a phosphoric ester was realized with a cyclodextrin-based catalyst (Figure 1-3).[4b] This is an excellent example of the combination of a molecular recognition site and a catalytically active site, however, the active sites were out of the nano-space due to the small capacity of the molecular host, which often caused undesired side reactions.

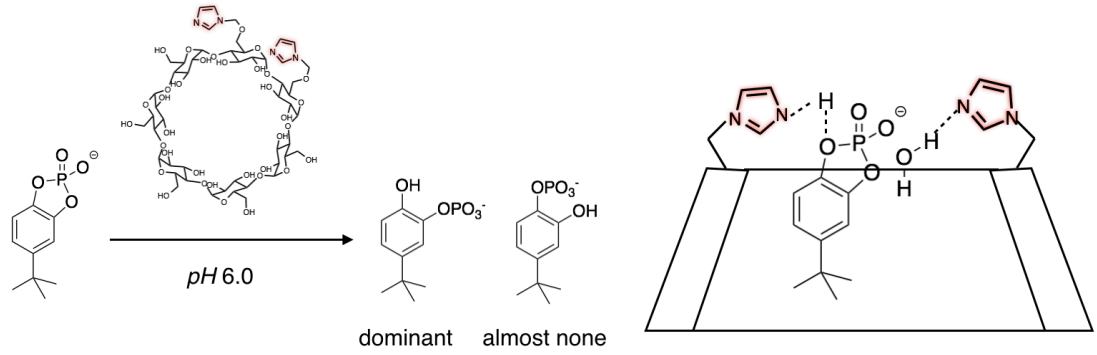

Figure 1-3. Cyclodextrin-based catalyst for the regio-selective hydrolysis of a phosphoric ester.[4b] The encapsulation of hydrophobic moiety in *β*-CD to regulate the relative position of each substrate for the regio-selective reaction.

Interestingly, several reactions were also catalyzed in some confined nano-spaces even without catalytically active sites.[5] For instance, a Zn^{II}-porphyrin-based molecular host can bring a diene close to a dienophile through coordination at its Zn centers to catalyze an *exo*-selective Diels-Alder reaction (Figure 1-4).[5b] It clearly indicated that the regulation of the spatial arrangement of reaction substrates in the confined spaces was important to realize highly selective reactions.

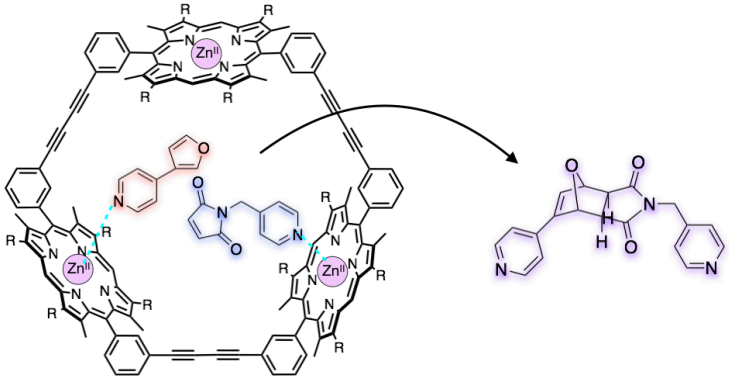

Figure 1-4. *Exo*-selective Diels-Alder reaction in a porphyrin cage.[5b] The coordination of reaction substrates on the Zn centers of the molecular host could regulate the spatial arrangement for the *exo*-selective reaction.

The introduction of active sites in artificial nano-spaces has also been examined through encapsulation derived from electronic interactions and immobilization *via* coordination and covalent bonding. One of the unique examples is encapsulation of metal catalysts in nano-spaces, and some of them showed remarkable effects of confined spaces in terms of the reaction rate, selectivity, and specificity.[6] For instance, a Rh catalyst in a Ga_4L_6 coordination cage exhibited size-specific reactivity for the isomerization of allyl alcohols (Figure 1-5).[6b] The bulky molecules could not access to the active site in the cage to result in the size-specific reaction.

As shown in the examples, the concept with respect to the active sites in confined spaces underlies in artificial catalytic systems, however, it is still challenging to precisely arrange active sites and substrates simultaneously in a single isolated nano-space.

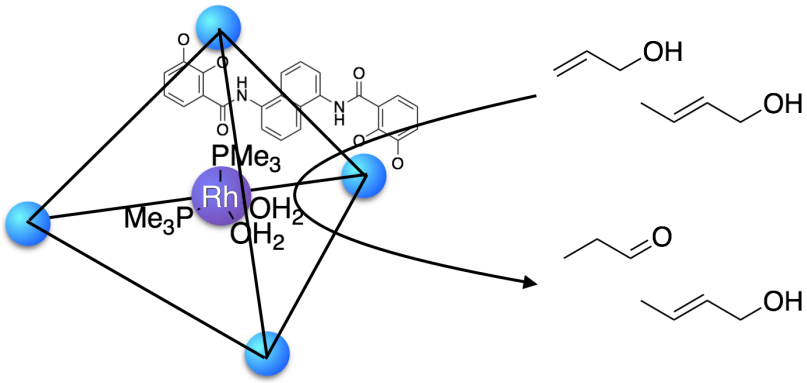

Figure 1-5. Size-specific reaction catalyzed by a Rh catalyst encapsulated in a Ga_4L_6 coordination cage.[6b] Only less bulky substrates underwent an oxidation reaction due to the spatial effect of the cage.

1-3. Metal–Organic Frameworks directed toward enzyme-like catalysts

In these several decades, a new type of porous materials, metal–organic frameworks (MOFs), have been developed and explosively spread because of the unique features such as gas storage, molecular separation, and catalysis.[7] MOFs are constructed from organic and inorganic components, which can afford a wide variety of MOFs based on the combination of the components (Figure 1-6). In addition to the construction of MOFs, the modification methods like post-synthetic modification have been well established.[8] Both the organic and inorganic parts can be modified to add extra functionalities to the original three-dimensional frameworks, which afforded tremendously wide platforms for various applications.

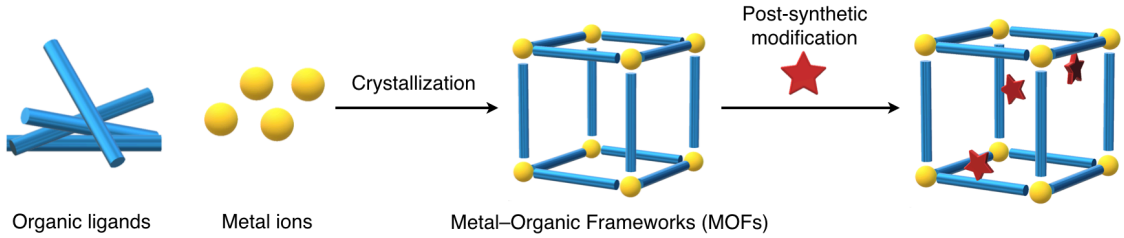

Figure 1-6. Schematic representation of the construction and post-synthetic modification of metal–organic frameworks (MOFs).

Therefore, a wide variety of MOFs with unique properties have been designed and developed. In particular, the utilization for catalysis is one of the most attractive targets because MOFs can provide designed nano-spaces, which play important roles in controlling reactions like enzymes. For instance, CMOF-1 was constructed from organic ligands with a chiral phosphoric acid, which works as an active site for an asymmetric catalytic reaction.[9a] The enantio-selectivity of the reaction in CMOF-1 became opposite due to the spatial effect of the rigid framework compared with the ligand-based catalyst (Figure 1-7). This example could show the possibility to regulate reactions in the nano-space of MOFs based on the strategy of active sites in confined spaces.

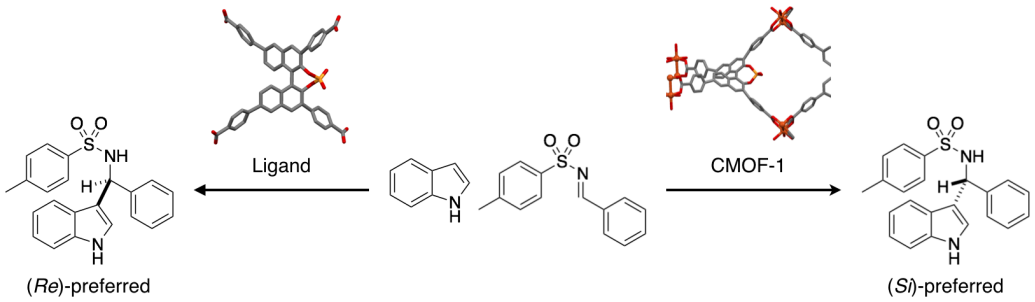

Figure 1-7. A typical example of the regulation of selectivity in MOF; cavity-induced reversal of enantio-selectivity in CMOF-1.[9a]

Regardless of these great achievements in the constructions, modifications and applications, enzyme-like catalyst based on MOFs has not been realized due to the difficulty in the site-selective arrangement of the active sites in the nano-spaces, which is essential to realize perfect specificity and selectivity like enzymes. A few examples of incorporation of multiple functionalities into the MOFs have been reported, but it is still very difficult to precisely arrange them in a single unit-space (Figure 1-8).[10]

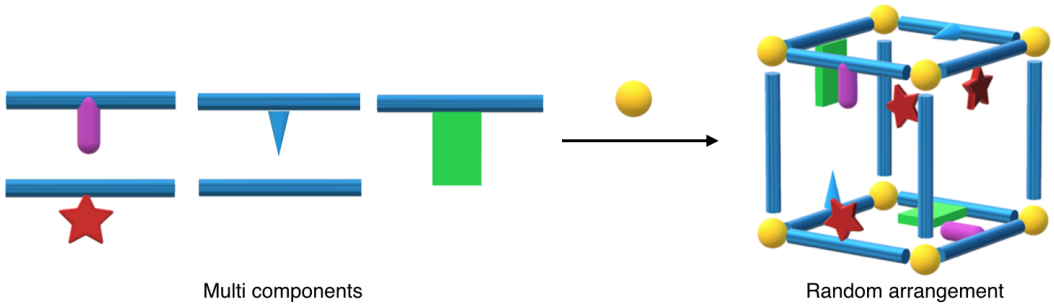

Figure 1-8. The random arrangement of multiple components.[10a]

As a new direction, molecular recognition ability was introduced in the nano-space of MOFs using macrocycle-based ligands.[11] For example, P5A-MOF-1 composed of a pillar[5]arene-based ligand can recognize several cationic liner molecules in the pillar[5]arene part (Figure 1-9). However, the simultaneous introduction of active sites for selective reaction was not achieved due to the difficulty of precise arrangement of multiple functionalities. Therefore, it is still challenging to construct well-defined nano-spaces in MOFs toward catalysts comparable to natural enzymes.

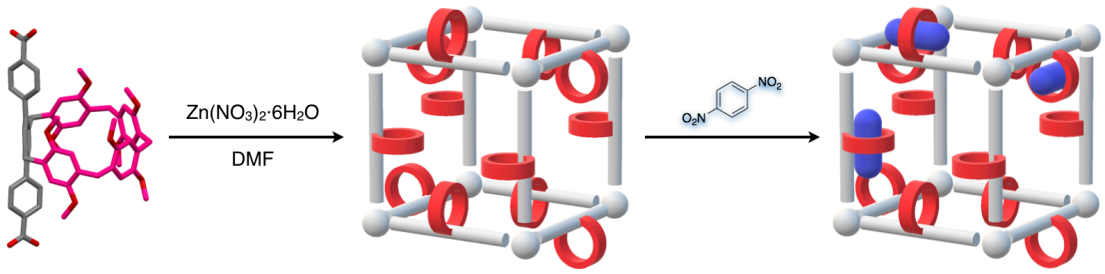

Figure 1-9. Molecular recognition ability based on the pillar[5]arene-based organic ligands.[11d]

1-4. Metal–Macrocycle Framework (MMF)

Recently, a porous molecular crystal, metal–macrocycle framework (MMF), has been developed in our laboratory. MMF was constructed from four isomers of trinuclear Pd^{II} complexes of macrocyclic hexamine **L** (Figure. 1-10).[12] The four isomers were divided into two helical isomers, *M* and *P*, which were derived from the direction of intramolecular CH-π interactions, and also divided into two conformational isomers, *syn* and *anti*, which were derived from the position of Pd^{II} centers. In the presence of three equivalents of $PdCl_2(CH_3CN)_2$ in acetonitrile, the four isomers equally formed and assembled by the Pd-Pd interactions, hydrogen bonding, and CH-π interactions to form porous MMF crystals with nano-channels arranged parallel to each other. On the other hand, a different solvent system (dichloromethane-DMSO) led to the formation of different porous crystals composed of only *syn*-isomers.[12e] In my research, I only focused on the former MMF crystals formed in acetonitrile.

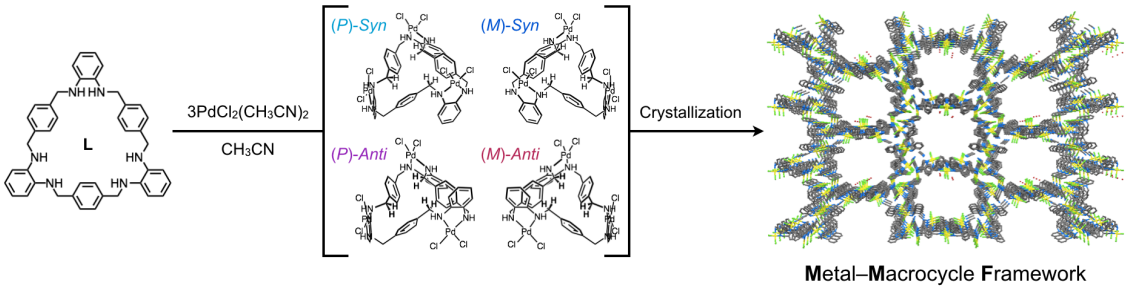

Figure 1-10. Construction of metal–macrocycle framework (MMF) composed of four isomers of trinuclear Pd^{II} complex with macrocyclic ligand **L**.

MMF has one-dimensional nano-channels with a 1.4 × 1.9 nm^2 dimension, in which five enantio-paired molecular binding sites are arranged on the inner surface (Figure 1-11 a, b). Three pairs of the binding sites are derived from the central pockets of macrocyclic complexes (pockets 1, 2, and 3), and the other two sets of the binding sites are derived from the interstitial void between the complexes (voids 4 and 5). Each binding site can entrap various guest molecules depending on the interactions between guest molecules and the frameworks. For example, *m*- and *p*-dibromobenzene molecules were shape-selectively adsorbed to different binding sites, (*S*)-1-(3-chlorophenyl)-1-ehtanol was diastereo-selectively adsorbed to one of the enantiomeric pockets, and the three different molecules were simultaneously and cooperatively adsorbed through the interactions with the binding sites (Figure 1-11 c-e).[11c] In addition, MMF has great potential to analyze dynamic molecular behaviors of guest molecules in the MMF nano-space by single-crystal XRD

measurement. For instance, the transient molecular adsorption behavior was visualized by an X-ray snapshot technique (Figure 1-12).[11d]

Based on these abilities, MMF has an excellent platform as precisely designed reaction nano-spaces and to analyze molecular behaviors and reactions in the nano-channel. However, the utilization of reaction nano-spaces had not been achieved because of the lack of catalytically active sites in the MMF nano-channel. Although there are exposed $PdCl_2$ centers, the Pd sites are too inert to catalyze reactions under common conditions due to its electronic structure and steric environment. Therefore, introduction of active sites was essential to utilize MMF as catalytic reaction sites.

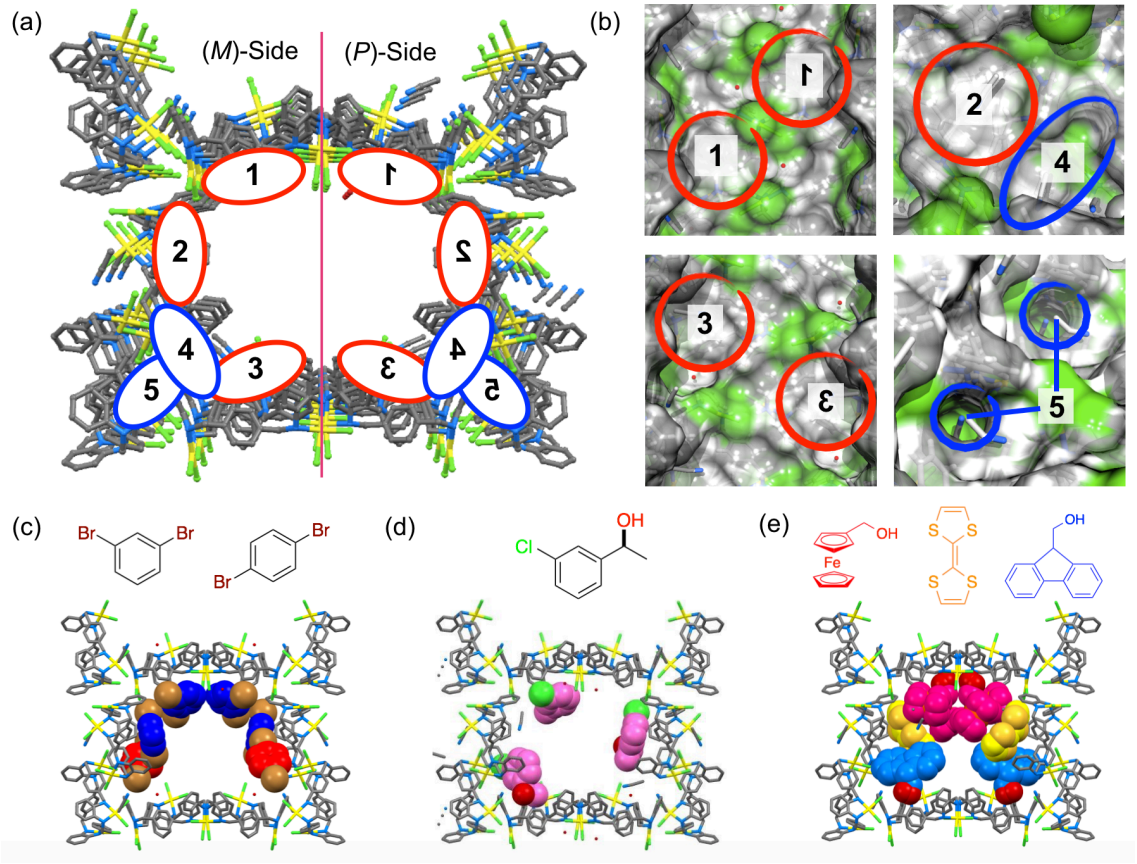

Figure 1-11. Structure of MMF nano-channel with molecular binding sites and their molecular binding abilities.[12a,b,c] (a) Five enantio-paired molecular binding sites in a nano-channel. 1) Upper pocket, 2) side pocket, 3) bottom pocket, 4) corner void, and 5) tubular void. (b) Solvent exclusive pore surfaces around each binding site. (c) Shape-selective adsorption of *meta*- and *para*-dibromobenzenes. (d) Diastereo-selective adsorption of (*S*)-1-(3-chlorophenyl)-1-ethanol. (e) Cooperative adsorption of hydroxymethyl ferrocene, tetrathiafluvalene (TTF), and 9-fluorenylmethanol.

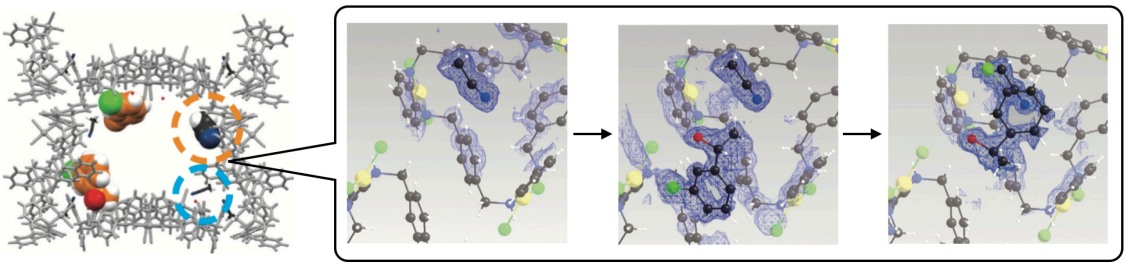

Figure 1-12. X-ray snapshot analysis of transient molecular adsorption in MMF nano-channel.[12d]

In the end of this section, I defined a word "unit-space" as a half of the unit-cell with one void space, which was constructed from one set of four isomers of Pd^{II}-trinuclear complexes (Figure 1-13).

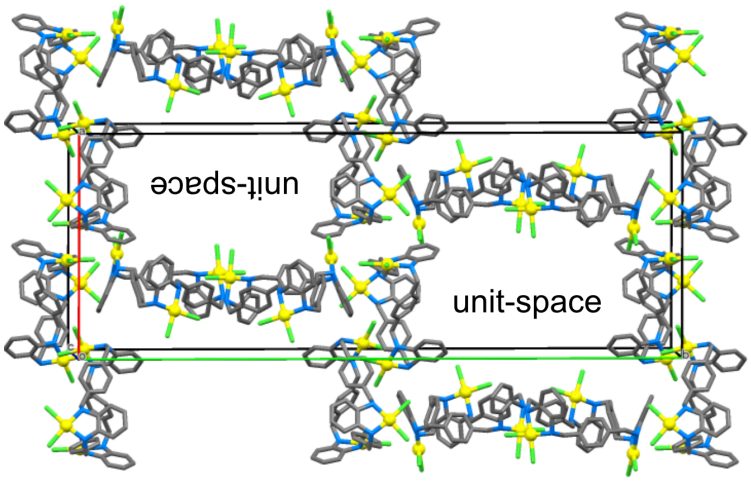

Figure 1-13. Definition of "unit-space". The box indicates a unit-cell of crystal structure, which includes two void spaces named "unit-space".

1-5. The aim of this study

The structures of enzymes, which include active sites in confined nano-spaces, have inspired chemists to develop supramolecular catalysts toward highly efficient and selective reactions as seen in natural enzymes. Some of the trials based on the strategy realized reactions with high selectivity and specificity. For example, the nano-space constructed in MOFs achieved a cavity-induced enantio-selective reaction. However, the enantiomeric excess was moderate because the spatial arrangement of the active sites was not regulated, and the molecular recognition sites required for highly selective reactions were not introduced in the framework. Therefore, it is still challenging to precisely design nano-spaces toward enzyme-like catalysts by the site-selective introduction of catalytically active sites in confined nano-spaces with molecular recognition ability. In this context, MMF is a promising candidate to develop enzyme-like catalysts based on the intrinsic multiple and simultaneous molecular recognition ability. However, the utilization of a reaction nano-space had not been realized because of the lack of active sites in the MMF nano-space. Therefore, it is a promising way to construct well-defined reaction nano-spaces by the introduction of active sites in the MMF nano-space for highly efficient and selective reactions (Figure 1-14).

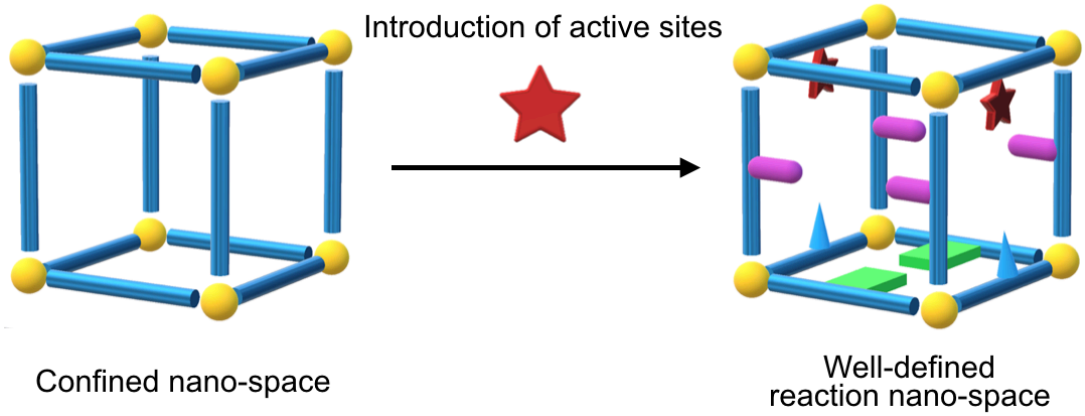

Figure 1-14. The concept of this study: introduction of active sites in a confined nano-space to construct a well-defined reaction nano-space for highly efficient and selective reactions.

In this research, I aimed to construct a well-defined reaction nano-space in the MMF channel by introduction of catalytically active sites. The introduction of active sites was examined in two approaches, adsorption of catalysts and activation of $Pd^{II}Cl_2$ centers in the framework. In addition, the unique reactivity of the Pd^{II} centers in the nano-space was discussed focusing on the spatial properties of the MMF nano-spaces.

This thesis consists of five chapters as follows (Figure 1-15):

Chapter 1 explains the background of the construction of functional nano-spaces, and describes a concept of the introduction of active sites in confined nano-spaces.

Chapter 2 describes the introduction of active sites by the adsorption of a homogeneous acid catalyst to realize a size-specific reaction based on the channel size of MMF.

Chapter 3 shows another approach to introduce active sites through the photo-activation of inert $Pd^{II}Cl_2$ centers in the framework to realize Pd^{II}-catalyzed olefin migration reactions.

Chapter 4 represents a preferential photoreaction in MMF, photo-induced olefin migration over intramolecular [2+2] cycloaddition. The spatial effects of the MMF nano-space on the inhibition of [2+2] cycloaddition are discussed from the viewpoint of molecular mobility as well as photo-shielding effect.

Chapter 5 describes conclusion of this study and future perspectives of precisely designed MMF nano-spaces to utilize as unique reaction nano-spaces for highly efficient and selective reactions.

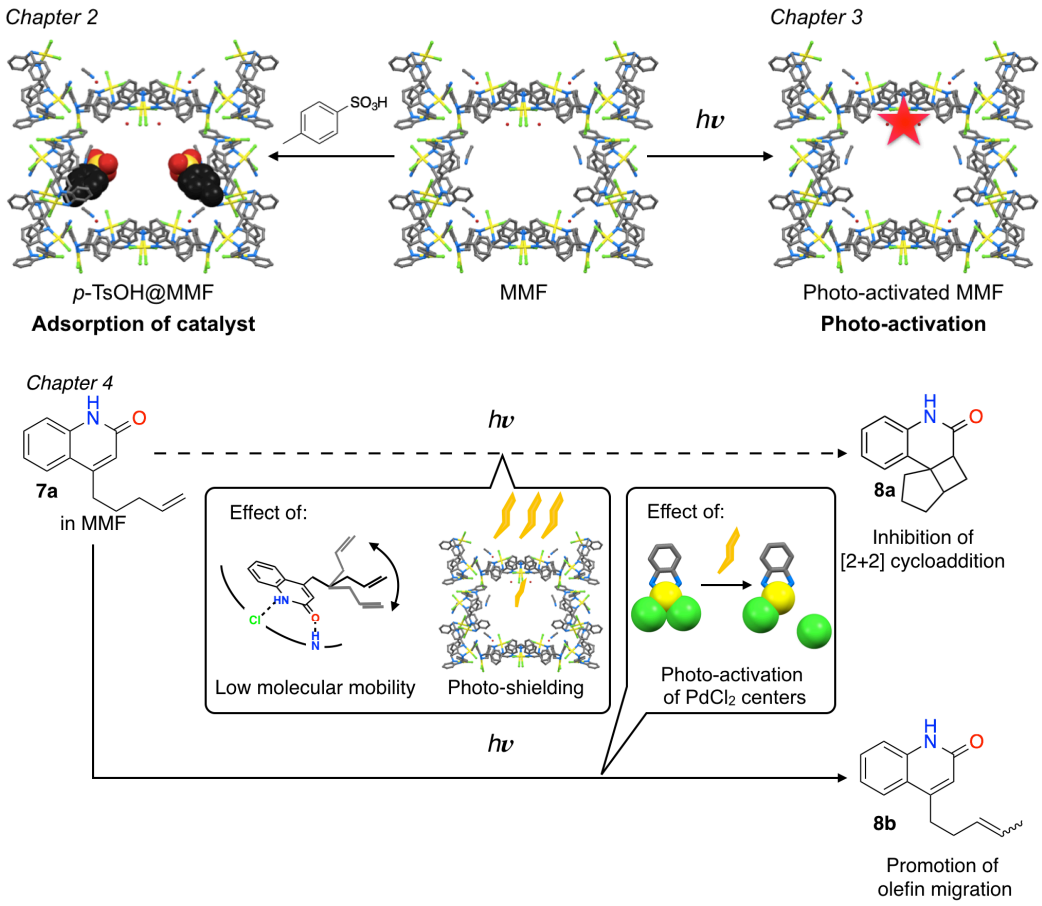

Figure 1-15. Schematic representation of each chapter (Chapters 2-4): the construction of reaction nano-spaces in MMF by two approaches and the discussion about the spatial effects of the MMF nano-space on the catalytic reactivity.

1-6. References

[1] (a) K. E. Neet, *J. Biol. Chem.* **1998**, *273*, 25527-25528. (b) E. Z. Eisenmesser, D. A. Bosco, M. Akke, D. Kern, *Science* **2002**, *295*, 1520-1523. (c) M. Shionoya (Ed.), "D. Rehder, *Bioinorganic Chemistry*", Tokyokagakudoujin, **2017**.

[2] (a) S. Takahashi, K. Okayama, S. Kunugi, K. Oda, *Biosci. Biotech. Biochem.* **1996**, *60*, 1651-1654. (b) A. de Kreij, G. Venema, B. van den Burg, *J. Biol. Chem.* **2000**, *275*, 31115-31120. (c) G. Parkin, *Chem. Rev.* **2004**, *104*, 699-767. (d) K. Oda, T. Takahashi, K. Takada, M. Tsunemi, K. K.-S. Ng, K. Hiraga, S. Harada, *FEBS Lett.* **2005**, *579*, 5013-5018. (e) O. A. Adekoya, I. Sylte, *Chem. Biol. Drug Des.* **2009**, *73*, 7-16.

[3] (a) R. Breslow, *Acc. Chem. Res.* **1995**, *28*, 146-153. (b) D. J. Cram, Angew. *Chem. Int. Ed. Engl.* **1988**, *27*, 1009-1020. (c) D. M. Vriezema, M. C. Aragonès, J. A. A. W. Elemans, J. J. L. M. Cornelissen, A. E. Rowan, R. J. M. Nolte, *Chem. Rev.* **2005**, *105*, 1445-1489. (d) T. S. Koblenz, J. Wassenaar, J. N. H. Reek, *Chem. Soc. Rev.* **2008**, *37*, 247-262. (e) M. Raynal, P. Ballester, A. Vidal-Ferran, P. W. N. M. van Leeuwen, *Chem. Soc. Rev.* **2014**, *43*, 1734-1787. (f) S. H. A. M. Leenders, R. Gramage-Doria, B. de Bruin, J. N. H. Reek, *Chem. Soc. Rev.* **2015**, *44*, 433-448.

[4] (a) R. Breslow, P. Campbell, *J. Am. Chem. Soc.* **1969**, *91*, 3085. (b) E. Anslyn, R. Breslow, *J. Am. Chem. Soc.* **1989**, *111*, 5972-5973.

[5] (a) J. Kang, J. Rebek Jr., *Nature* **1997**, *385*, 50-52. (b) Z. Clyde-Watson, A. Vidal-Ferran, L. J. Twyman, C. J. Walter, D. W. J. McCallien, S. Fanni, N. Bampos, R. S. Wylie, J. K. M. Sanders, *New. J. Chem.* **1998**, *22*, 493-502. (c) M. Yoshizawa, M. Tamura, M. Fujita, *Science* **2006**, *312*, 251-254.

[6] (a) A. W. Kleij, J. N. H. Reek, *Chem. Eur. J.* **2006**, *12*, 4218-4227. (b) D. H. Leung, R. G. Bergman, K. N. Raymond, *J. Am. Chem. Soc.* **2007**, *129*, 2746-2747.

[7] (a) S. Kitagawa, R. Kitaura, S. Noro, *Angew. Chem. Int. Ed.* **2004**, *43*, 2334-2375. (b) S. Kitagawa, R. Matsuda, *Coord. Chem. Rev.* **2007**, *251*, 2490-2509. (c) H. Furukawa, K. E. Cordova, M. O'Keeffe, O. M. Yaghi, *Science* **2013**, *341*, 1230444.

[8] (a) K. K. Tanabe, S. M. Cohen, *Chem. Soc. Rev.* **2011**, *40*, 498-519. (b) P. Deria, J. E. Mondloch, L. Karagiaridi, W. Bury, J. T. Hupp, O. K. Farha, *Chem. Soc. Rev.* **2014**, *43*, 5896-5912. (c) S. M. Cohen, *J. Am. Chem. Soc.* **2017**, *139*, 2855-2863.

[9] (a) M. Zheng, Y. Liu, C. Wang, S. Liu, W. Lin, *Chem. Sci.* **2012**, *3*, 2623-2627. (b) L. Li, R. Matsuda, I. Tanaka, H. Sato, P. Kanoo, H. J. Jeon, M. L. Foo, A. Wakamiya, Y. Murata, S. Kitagawa, *J. Am. Chem. Soc.* **2014**, *136*, 7543-7546.

[10] (a) H. Deng, C. J. Doonan, H. Furukawa, R. B. Ferreira, J. Towne, C. B. Knobler, B. Wang, O. M. Yaghi, *Science* **2010**, *327*, 846-850. (b) L. J. Wang, H. Deng, H. Furukawa, F. Gandara, K. E. Cordova, D. Peri, O. M. Yaghi, *Inorg. Chem.* **2014**, *53*, 5881-5883. (c) M. L. Foo, R. Matsuda, S. Kitagawa, *Chem. Mater.* **2014**, *26*, 310-322.

[11] (a) S. Tashiro, M. Shionoya, *Bull. Chem. Soc. Jpn.* **2014**, *87*, 643-654. (b) H. Zhang, R. Zou, Y. Zhao, *Coord. Chem. Rev.* **2015**, *292*, 74-90. (c) Q. Li, W. Zhang, O. S. Miljanic, C.-H. Sue, Y.-L. Zhao, L. Liu, C. B. Knobler, J. F. Stoddart, O. M. Yaghi, *Science* **2009**, *325*, 855-859. (d) N. L. Strutt, D. Fairen-Jimenez, J. Iehl, M. B. Lalonde, R. Q. Snurr, O. K. Farha, J. T. Hupp, J. F. Stoddart, *J. Am. Chem. Soc.* **2012**, *134*, 17436-17439. (e) R. Haldar, R. Matsuda, S. Kitagawa, S. J. George, T. K. Maji, *Angew. Chem. Int. Ed.* **2014**, *126*, 11966-11971.

[12] (a) S. Tashiro, R. Kubota, M. Shionoya, *J. Am. Chem. Soc.* **2012**, *134*, 2461-2464. (b) R. Kubota, S. Tashiro, T. Umeki, M. Shionoya, *Supramol. Chem.* **2012**, *24*, 867-877. (c) S. Tashiro, T. Umeki, R. Kubota, M. Shionoya, *Angew. Chem. Int. Ed.* **2014**, *136*, 17946-17949. (d) R. Kubota, S. Tashiro, M. Shiro, M. Shionoya, *Nat. Chem.* **2014**, *6*, 913-918. (e) R. Kubota, S. Tashiro, M. Shionoya, *Chem. Sci.* **2016**, *7*, 2217-2221.

Chapter 2

Non-covalent immobilization of an acid catalyst for a size-specific reaction

2-1. Introduction

Immobilization of homogeneous catalysts to the inner surface of porous materials can provide reaction spaces to realize efficient and selective reactions based on heterogeneous catalysis. The nanoporous materials with a uniform structure have great advantages of well-defined space-specific reactions different from polymer supports or amorphous solids.

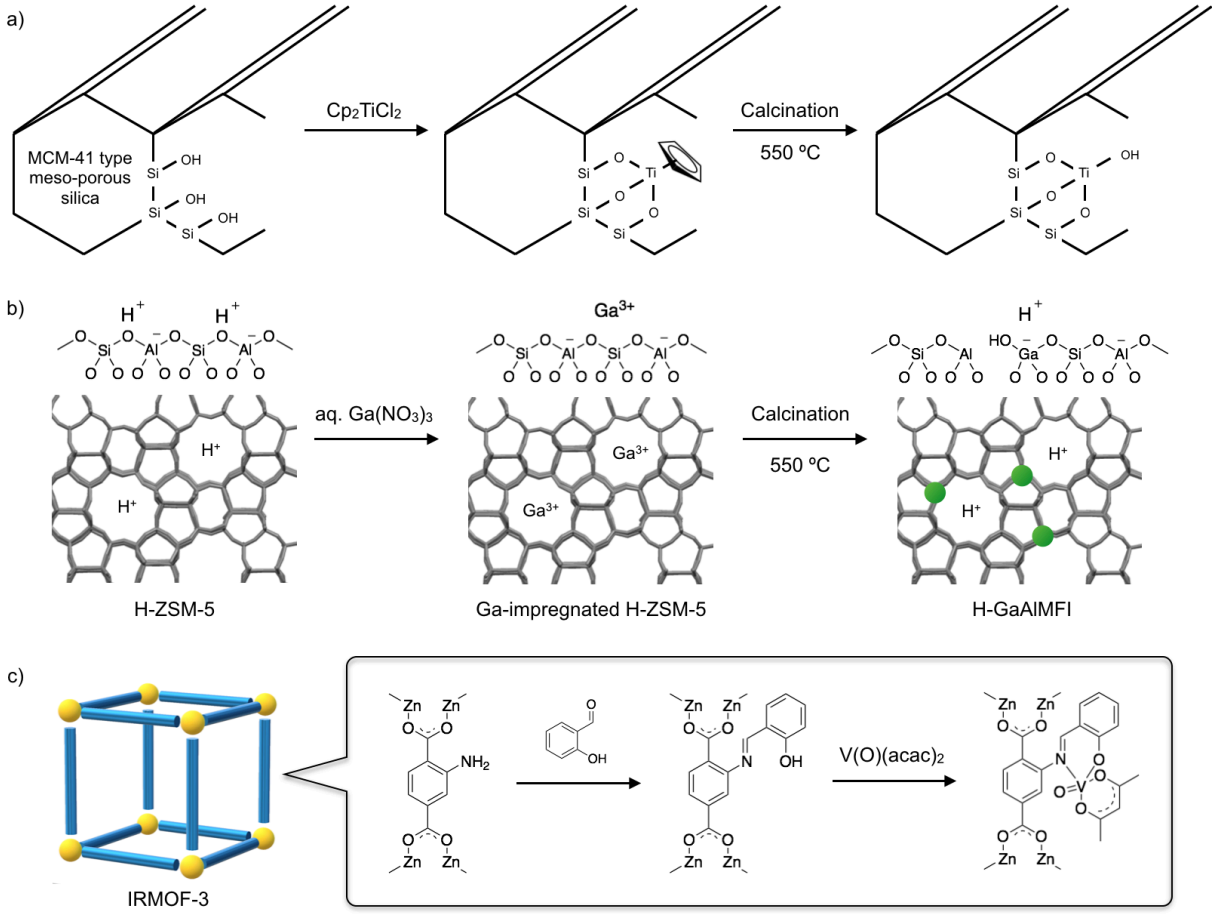

Figure 2-1. Early examples of the introduction of active sites in porous materials. (a) Grafting of titanocene dichloride in meso-porous silica.[6a] (b) Impregnation of Ga ions and successive incorporation into the framework of zeolite.[7a] (c) Post-synthetic modification by organic and inorganic functionalities.[8b]

In these several decades, the development of porous materials such as zeolite,[1] meso-porous silica,[2] and metal-organic frameworks (MOFs)[3] and their derivatives[4] has prompted us to construct a variety of confined nano-spaces. In addition, various chemical modification methods of these materials enabled us to modify the nano-spaces with extra functionalities to utilize for space-specific reactions.[5] Typical examples are as follows; (1) grafting functional molecules by covalent bonding for modification of meso-porous silica

(Figure 2-1a),[6] (2) the cation exchange with reactive metal cations and successive incorporation into the frameworks for zeolite (Figure 2-1b),[7] and (3) functionalization of the frameworks by both organic and inorganic functionalities as active sites for MOFs (Figure 2-1c).[8] In these chemical modifications, the covalent modification is a powerful tool to construct robust reaction nano-spaces, but non-covalent modification such as adsorption of a catalyst to the inner space is also an excellent way when the catalyst has an affinity to a certain molecular recognition site of the inner space in terms of the simple preparation and exchangeability. Therefore, porous materials with inner molecular recognition sites have great potential to provide an excellent platform for highly controlled reaction fields.[9]

A porous molecular crystal, metal–macrocycle framework (MMF), has great potential to serve as well-defined reaction nano-spaces possessing molecular recognition sites on the inner surfaces.[10] A wide range of molecules are known to be adsorbed to a certain binding site depending on the preferable non-covalent interactions between guest molecules and the inner surfaces. Inspired by this molecular binding ability, I envisioned construction of reaction nano-space with a well-defined dimension that would allow space-specific reactions based on the site-selective adsorption of a homogeneous catalyst. The simple operations of soaking and washing could provide a reusable heterogeneous acid catalyst.

2-2. Immobilization of *p*-TsOH in MMF

Introduction of active sites in the MMF nano-space was examined with *p*-toluenesulfonic acid (*p*-TsOH) because this molecule is a typical acid catalyst and its adsorbed structure in MMF has been determined.[10b] However, the adsorption behaviors such as encapsulation kinetics, stability, and solvent tolerance in MMF have not been investigated, and their studies are essential to optimize stable immobilization of *p*-TsOH in MMF. In this section, the preparation of *p*-TsOH@MMF, in which *p*-TsOH is stably immobilized in MMF, and analyses of encapsulation and desorption of *p*-TsOH by digestion NMR and single-crystal XRD experiments are described.

2-2-1. Encapsulation behaviors of *p*-TsOH into MMF

Encapsulation behaviors of *p*-TsOH into MMF were assessed by ^{1}H NMR time-course analysis. After soaking MMF crystals in an acetonitrile solution of *p*-TsOH·H_2O (0.80 M) for a fixed time, the resulting MMF crystals were collected to conduct digestion NMR experiments (Scheme 2-1), that is ^{1}H NMR analyses of digested MMF crystals in DCl/DMSO-d_6 solutions to estimate the number of encapsulated *p*-TsOH molecules in a unit-space of MMF. The number of encapsulated molecules was calculated from the integral ratio of ^{1}H NMR peaks of *p*-TsOH molecules to those of the protonated macrocyclic ligands $[\mathbf{L} + n\ \mathrm{H}]^{n+}$.

Scheme 2-1. Schematic representation of a digestion NMR experiment to determine the number of *p*-TsOH molecules in a unit-space of MMF.

The signals of *p*-TsOH at 7.5, 7.2, and 2.3 ppm became larger as the soaking time advanced, but became saturated within one hour. This result indicated that the number of encapsulated *p*-TsOH increased as the soaking time advanced (Figures 2-2, 2-3), and the molecules were equally dispersed in the whole channel at the saturated level. Eventually, the MMF crystals including *ca*. 5 *p*-TsOH molecules per a unit-space could be obtained.

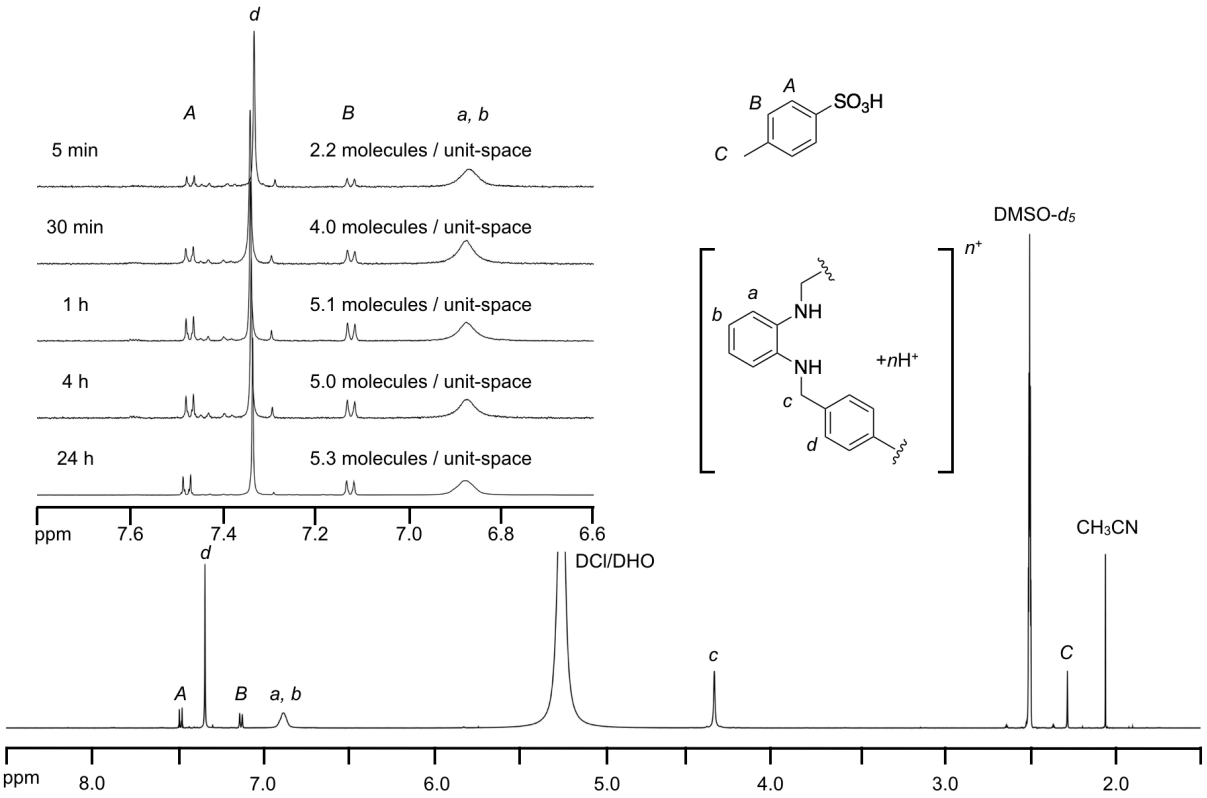

Figure 2-2. ^{1}H NMR spectra of digestion NMR experiments (500 MHz, DCl/DMSO-d_6, 300 K). The inset shows the time-course of encapsulation. The time on the left side of each spectrum indicates the total soaking time. The estimated numbers of *p*-TsOH molecules encapsulated in a unit-space of MMF are shown on the right side.

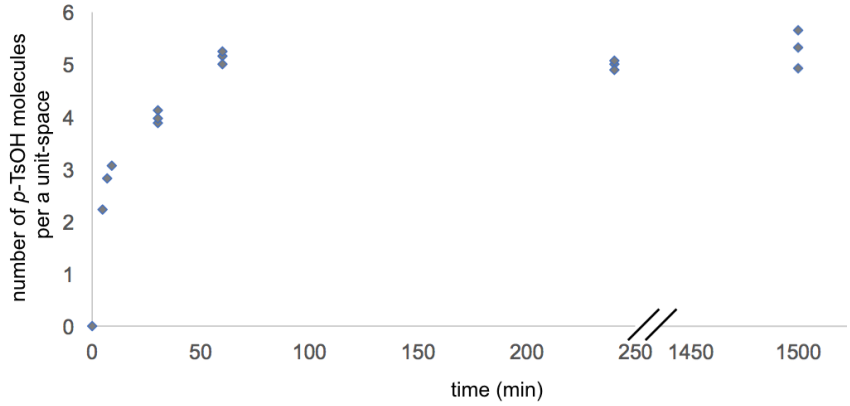

Figure 2-3. The time-course of the encapsulation of *p*-TsOH molecules into MMF. The number of *p*-TsOH molecules per a unit-space was estimated by the digestion NMR experiments.

Single-crystal X-ray analysis of the resulting MMF crystal including *ca.* 5 *p*-TsOH molecules was also conducted to reveal the adsorbed structure of *p*-TsOH molecules in the MMF nano-space. As previously reported, *p*-TsOH molecules were adsorbed to two binding sites with non-covalent interactions such as CH-π

interactions, and the number of adsorbed molecules per a unit-space could be estimated to be approximately one (Figure 2-4, *ca.* 50% occupancy × two binding sites). Even after soaking for 1 h, the occupancy of *p*-TsOH molecule was not changed so that the adsorption process appeared to reach the equilibrium state within 1 h. Since the encapsulation of *ca*. 5 molecules per a unit-space was suggested by digestion NMR experiments, *ca*. 4 molecules per a unit-space should be disordered in the void space, but not adsorbed on the surface of the inner space. Therefore, non-adsorbed *p*-TsOH should be excluded to eliminate a background reaction derived from excess *p*-TsOH.

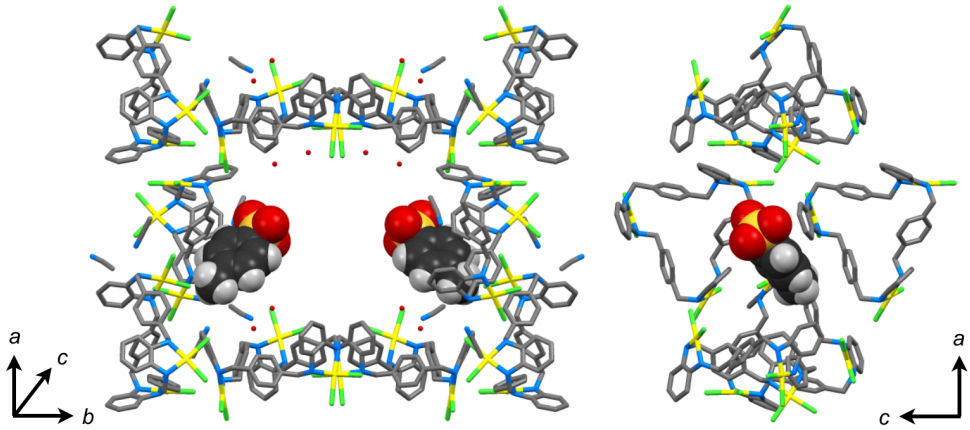

Figure 2-4. Crystal structure of MMF including *ca.* 5 *p*-TsOH molecules. The *p*-TsOH molecules were adsorbed onto the corner voids with *ca.* 50% occupancy. The other *ca.* 4 *p*-TsOH molecules should be disordered in the channel space.

2-2-3. Establishment of washing procedure

With a decrease in the number of molecules in the MMF, adsorbed *p*-TsOH molecules would be dissociated from the inner surface, because the adsorption of *p*-TsOH depends on the concentration of the molecule. However, if the solvent filled in the nano-space was replaced with a poor solvent for *p*-TsOH, desorption of adsorbed molecules could be suppressed due to the change in the equilibrium state. Based on this idea, MMF crystals including *ca.* 5 *p*-TsOH molecules were washed by soaking in pure solvents. Three kinds of solvents were tested as below; acetonitrile as a good solvent (up to 0.8 M soluble), dichloromethane as a poor solvent (up to 1 mM), and *n*-hexane as a insoluble solvent (completely insoluble) for *p*-TsOH.

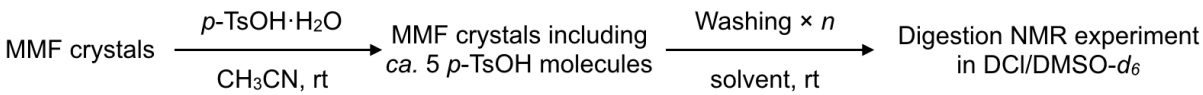

Scheme 2-2. Schematic representation of the protocol for digestion NMR experiments to analyze washing efficiency. Washing in pure solvent was repeated a few times (n = 0 ~ 3).

After the encapsulation of *p*-TsOH into MMF, the resulting crystals including *ca*. 5 molecules per a unit-space were soaked in each solvent (acetonitrile, dichloromethane, or *n*-hexane) for 12 h at 20 °C, and then collected to assess the efficiency of washing procedures. This washing operation was repeated three times in total. In each washing step, the number of *p*-TsOH kept in MMF was estimated by a digestion NMR experiment (Scheme 2-2).

The number of encapsulated *p*-TsOH molecules per a unit-space completely remained even after washing three times in *n*-hexane (Figure 2-5a), indicating no exclusion proceeded with *n*-hexane. In contrast, the number decreased to one or less by washing in acetonitrile (Figure 2-5b), which implied even adsorbed molecules were washed out. On the other hand, the number gradually decreased by washing in dichloromethane (Figure 2-5c), indicating adsorbed *p*-TsOH remained after washing three times. These results suggested the high dependence of washing efficiency on the solubility of *p*-TsOH.

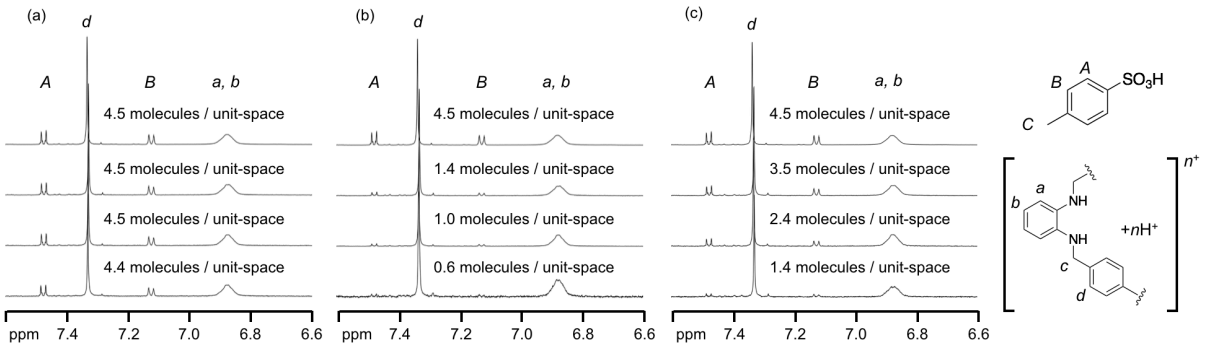

Figure 2-5. ^{1}H NMR spectra of digestion NMR experiments after each washing step with three types of solvents (500 MHz, DCl/DMSO-d_6, 300 K): washing in (a) *n*-hexane, (b) acetonitrile and (c) dichloromethane. The estimated number of *p*-TsOH molecules in a unit-space of MMF is shown on the right side for each spectrum. The spectra indicate those before washing, after the first, second, and third washing, starting from the top.

Based on the experiments, the washing condition in dichloromethane was optimized more precisely to establish a suitable washing procedure. For instance, the ratio of the volume of washing solvent and the weight of crystals was fixed to 1 mL/1 mg, and the filtration process was changed to decantation to avoid the degradation of crystals. After the first and second washing steps, the number of encapsulated molecules gradually decreased to 1.6 ± 0.1 molecules per a unit-space. However, after the third washing step, the number was kept 1.7 ± 0.2 molecules per a unit-space (Figure 2-6). This result suggested that only the adsorbed molecules on the inner surface remained in the MMF channel. Even the fourth washing kept the

number around 1.5 ± 0.1 molecules per a unit-space, indicating the stable immobilization of *p*-TsOH molecules in the MMF channel. Further washing in $CDCl_3$ was also examined considering the utilization as a heterogeneous catalyst in $CDCl_3$. The number of encapsulated molecules was almost unchanged to be 1.6 molecules per a unit-space, supporting the fact that *p*-TsOH molecules can be stably immobilized also in $CDCl_3$. The washing procedure was thus optimized, and the resulting heterogeneous acid catalyst including *ca.* 1.6 *p*-TsOH molecules per a unit-space was named *p*-TsOH@MMF.

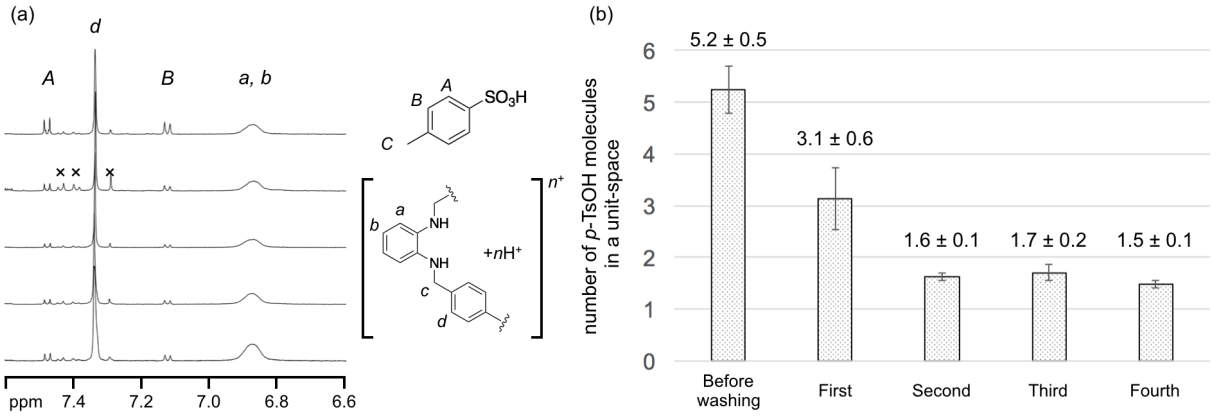

Figure 2-6. (a) ^{1}H NMR spectra of digestion NMR experiments after washing in dichloromethane (500 MHz, DCl/DMSO-d_6, 300 K). The spectra indicate those before washing, after the first, second, third, and forth washing, starting from the top. (b) The changes in the number of *p*-TsOH molecules in a unit-space of MMF before and after washing in dichloromethane. The data of three samples of the same batch are averaged, and the error bar represents twice of the standard deviation.

Single-crystal XRD measurement of *p*-TsOH@MMF was conducted to determine its structure. The crystallinity was almost maintained, though the quality of crystal was lowered a little judging from less peaks in the high-angle region. Unfortunately, *p*-TsOH molecules could not be observed in the crystal structure. Therefore, it still remains unclear whether it was due to the lower quality of crystal or to the heavy disorder in the MMF channel that *p*-TsOH molecules were not observed. Aside from this, it is apparent that excess *p*-TsOH molecules in the MMF channel were excluded through the optimized washing procedure, and that *p*-TsOH molecules are stably immobilized in $CDCl_3$ and can be used for catalytic reactions in *p*-TsOH@MMF.

2-3. Catalytic activity of *p*-TsOH@MMF

In this section, the catalytic activity of the prepared *p*-TsOH@MMF is described focusing on the size-specific hydrolysis reaction. The heterogeneous catalysis based on the stable immobilization of *p*-TsOH to the inner surface of MMF was examined in terms of the space-specificity, stability and efficiency of catalyst, leaching behaviors, and reusability due to the non-covalent immobilization, in comparison with normal homogeneous catalysis. As a goal of this study, a catalytic reaction with high size-specificity was realized by the reaction between a smaller $PhCH_2OCPh_3$ **1** and a larger Pd-$TPPCH_2OCPh_3$ **2**.

2-3-1. Hydrolysis of trityl group catalyzed by *p*-TsOH@MMF

The catalytic activity of *p*-TsOH@MMF (1.6 *p*-TsOH molecules per a unit-space) was examined by the hydrolysis reaction of $PhCH_2OCPh_3$ **1**. To a $CDCl_3$ solution of **1** (2.2 mM) was added *p*-TsOH@MMF (6 mol%) and the time-course analysis of the reaction was performed by ^1H NMR measurement. The water content, which worked as a reagent for this hydrolysis reaction, and the conversion of the reaction were estimated based on the internal standard $C_2H_2Cl_4$. The reaction was independently repeated three times to confirm the reproducibility. The encapsulation of **1** in the MMF channel was supported by a digestion NMR experiment in which *ca.* 0.2 molecules per a unit-space was encapsulated after one day soaking in a $CDCl_3$ solution of **1** (0.5 M).

(a)

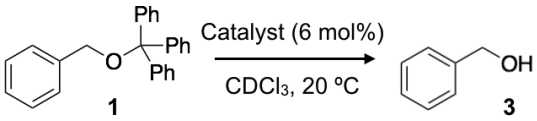

1 **3**

Entry	Catalyst	Time	Conversion (%)
1	*p*-TsOH@MMF	3 weeks	77
2	*p*-TsOH@MMF	3 weeks	71
3	*p*-TsOH@MMF	3 weeks	59

(b)

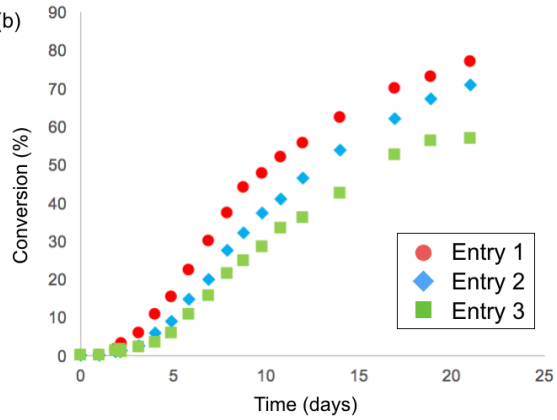

Figure 2-7. (a) The hydrolysis of **1** with *p*-TsOH@MMF in $CDCl_3$. (b) Time-course analysis of the reaction. The number of equivalent of the catalyst was estimated based on the number of *p*-TsOH molecules in *p*-TsOH@MMF. [**1**]: 2.2 mM. [H_2O]: 23 mM.

In all samples, the hydrolysis reaction did not proceed during the first two days, but then gradually proceeded for three weeks to produce benzyl alcohol in 77, 71, and 59% yields for the three experiments (Figures 2-7, 2-8). The shape of reaction profiles is similar in all entries, though there is a little range in yield. The induction period before the reaction starts and the later slow reaction may be due to the slow diffusion of **1** in the MMF channels to access adsorbed *p*-TsOH sites due to its large size.

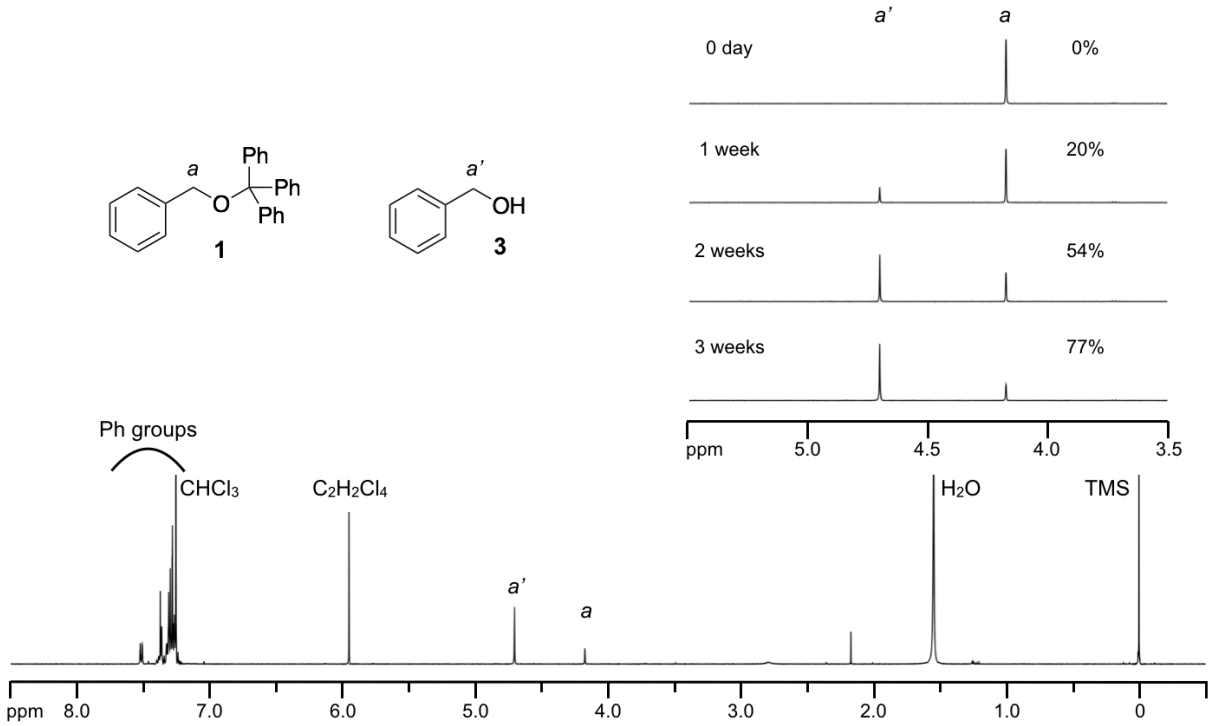

Figure 2-8. ^{1}H NMR spectra of the hydrolysis reaction with **1** (500 MHz, $CDCl_3$, 300 K) (entry 1 in Figure 2-7). The bottom spectrum indicates the full spectrum after three weeks, and the inset shows the time-course of the reaction in entry 1 of Figure 2-7a. The time on the left side of each spectrum indicates the total reaction time. The estimated conversion values are shown on the right side.

2-3-2. Elucidation of the catalytic species of *p*-TsOH@MMF

The catalytic activity of *p*-TsOH@MMF was compared with those of its components (*p*-TsOH·H_2O and MMF) to clarify the catalytic species of *p*-TsOH@MMF. One of the components was added to a $CDCl_3$ solution of **1** (*ca*. 2.0 mM), and the reaction mixture was analyzed by ^{1}H NMR spectroscopy.

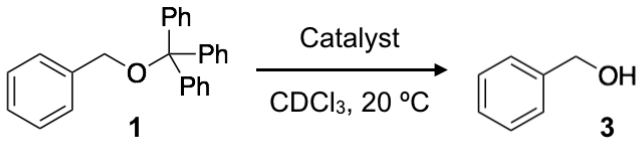

Entry	Catalyst	Time	Conversion (%)
1[a]	*p*-TsOH@MMF (6 mol%)[b]	3 weeks	69
2	*p*-TsOH·H_2O (5 mol%)	1.5 h	96
3	MMF (20 mol%)[c]	3 weeks	0

Scheme 2-3. Comparison of catalytic activities of *p*-TsOH@MMF and its components. [a)] The data of three experiments are averaged. [b)] The number of equivalent of the catalyst was calculated based on the number of *p*-TsOH molecules immobilized in *p*-TsOH@MMF. [c)] The number of equivalent of the catalyst was calculated based on the number of unit-space of MMF. [**1**]: 1.9–2.2 mM. [H_2O]: 23 mM.

When *p*-TsOH@MMF (6 mol%) was used as a catalyst, the reaction proceeded slowly, but finally yielded 69% conversion on average after three weeks (Scheme 2-3, entry 1). In the case of *p*-TsOH·H_2O (5 mol%), the hydrolysis smoothly proceeded and yielded 96% conversion in 1.5 h (entry 2). In contrast, MMF crystals showed no catalytic activity even after three weeks (entry 3). These results clearly indicate that only *p*-TsOH molecules work as a catalyst among all the components of *p*-TsOH@MMF. Moreover, a difference in the catalytic feature of *p*-TsOH@MMF from the homogeneous catalyst can be well explained by the stably immobilized *p*-TsOH in MMF. The much slower reaction in *p*-TsOH@MMF compared with the homogeneous reaction in the presence of *p*-TsOH·H_2O as the catalyst may be due to the slow diffusion of the reaction substrate in the MMF channel. If this assumption is correct, only the *p*-TsOH molecules adsorbed in the channels are the catalytic species in this reaction proceeded in the MMF channel.

2-3-3. Reusability of the catalyst *p*-TsOH@MMF

Next, the reusability of the heterogeneous catalytic activity of *p*-TsOH@MMF was assessed. After the first hydrolysis reaction of **1**, decantation and filtration of reaction mixtures were conducted to separate the solid catalyst, *p*-TsOH@MMF (used), from the supernatants. To the separated *p*-TsOH@MMF (used) was added a $CDCl_3$ solution of **1**, and the reaction was analyzed by ^1H NMR spectroscopy to examine the reusability (Scheme 2-4). Furthermore, the solid catalyst used twice was subjected to the digestion NMR experiments to confirm the number of *p*-TsOH molecules in the reused catalyst.

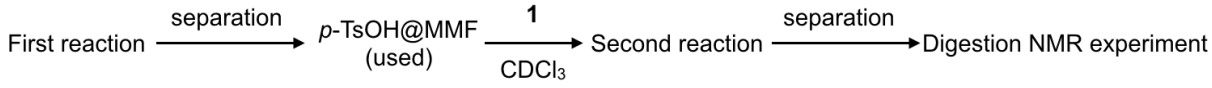

Scheme 2-4. Schematic representation of the protocol for reusability test.

The first hydrolysis reactions of **1** were conducted for three weeks at 20 °C and yielded 69% conversion on average (Scheme 2-5a). However, the second reactions with *p*-TsOH@MMF (used) did not show any catalytic activity even after three weeks at 20 °C. After additional three weeks at 50 °C, the reaction systems yielded 60% conversion on average (Scheme 2-5b). This result supported the reusability of *p*-TsOH@MMF, though the reactivity decreased. The decrease in the reactivity of *p*-TsOH@MMF (used) may be due to the slight decomposition of the channel window, which would disturb the diffusion of **1** into the reaction space. The crystal size became smaller after the reaction, suggesting slight decomposition of the channel window.

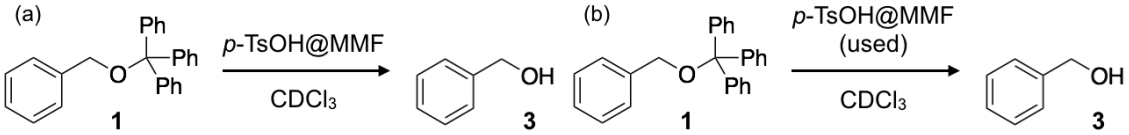

Entry	Condition	Conversion (%)
1	20 °C, 3 weeks	69

Entry	Condition	Conversion (%)
1	20 °C, 3 weeks	0
	+ 50 °C, 3 weeks	60

Scheme 2-5. (a) The first and (b) second reactions. The data of three batches are averaged. [**1**]: 2.0-2.2 mM. [H_2O]: 23 mM for (a) and 12 mM for (b). *p*-TsOH@MMF: 6 mol%. *p*-TsOH@MMF (used): 6 mol%. The equivalent of the catalyst was calculated based on the number of *p*-TsOH molecules immobilized in *p*-TsOH@MMF or *p*-TsOH@MMF (used).

After the second reaction, the reaction mixtures were filtrated, and the residual solid catalysts were submitted to digestion NMR experiments to assess the number of *p*-TsOH molecules remained in MMF. The number of remained *p*-TsOH molecules per a unit-space of MMF was estimated to 1.4 ± 0.2 molecules per a unit-space (Figure 2-9). This result is almost the same as *p*-TsOH@MMF as prepared (1.6 ± 0.2 molecules per a unit-space), which also supported the heterogeneous character of *p*-TsOH@MMF.

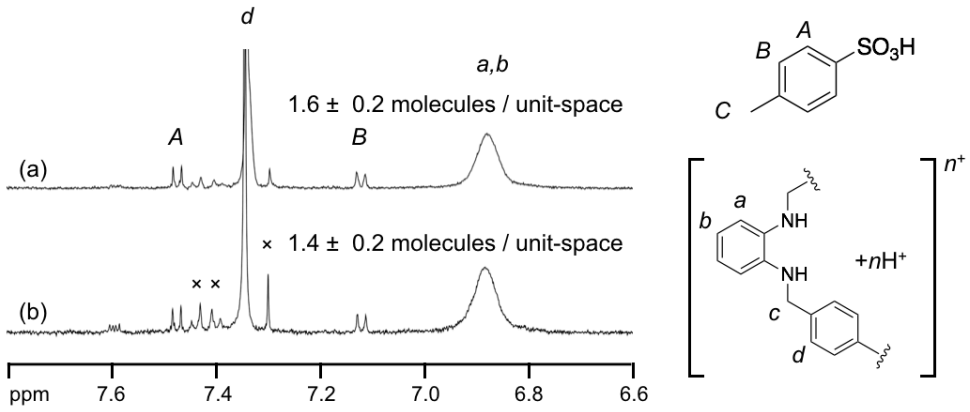

Figure 2-9. ^{1}H NMR spectra of digestion NMR experiment of *p*-TsOH@MMF (500 MHz, DCl/DMSO-d_6, 300 K): (a) as prepared and (b) after the second reaction. The numbers on the right sides indicate the average numbers of remained *p*-TsOH molecules per a unit-space of *p*-TsOH@MMF and twice of the standard deviation.

2-3-4. Leaching test

The heterogeneous property of *p*-TsOH@MMF was also assessed by a leaching test. The supernatants were separated from the reaction mixtures of the first and second reactions, and then a $CDCl_3$ solution of **1** was added to each supernatant, followed by ^{1}H NMR measurement (Scheme 2-6).

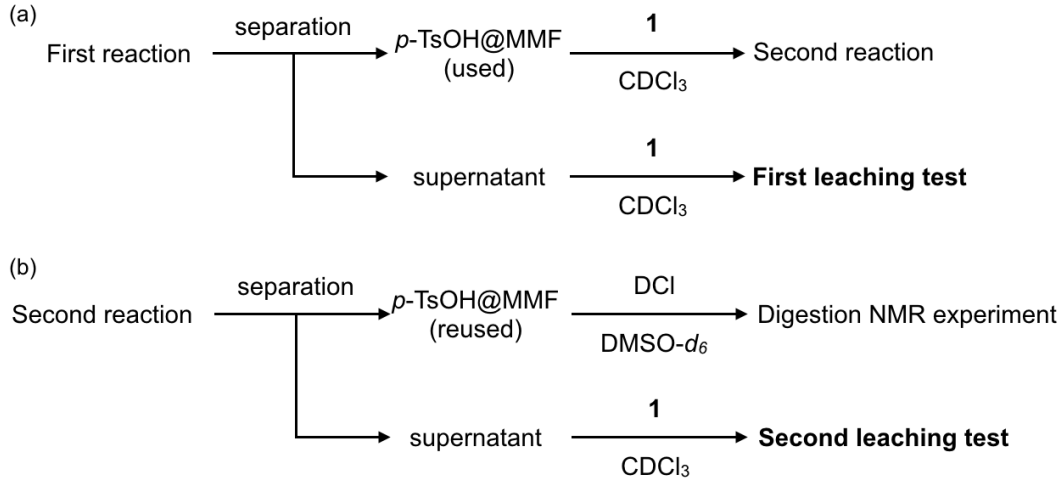

Scheme 2-6. Schematic representation of the protocol for the leaching tests. (a) The first leaching test for the first reaction. (b) The second leaching test for the second reaction.

The supernatants of the first reactions did not show any catalytic activity even after three weeks at 20 °C and heating at 50 °C (Scheme 2-7a). This result indicates that *p*-TsOH did not leach away from the channel during the first hydrolysis reactions. The leaching test was also conducted for the second reaction. The

supernatants of the second reactions also did not show any catalytic activity even after three weeks at 50 °C (Scheme 2-7b), indicating no leaching occurred during the second hydrolysis reactions.

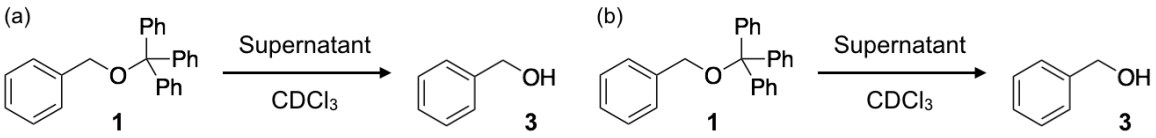

Entry	Condition	Conversion (%)
1	20 °C, 3 weeks	< 1
	+ 50 °C, 3 weeks	< 1

Entry	Condition	Conversion (%)
1	50 °C, 3 weeks	< 1

Scheme 2-7. (a) The first and (b) the second leaching tests. [H_2O]: 25 mM. $CDCl_3$ solutions of **1** (2.0 mM) was added to the supernatants of the hydrolysis reactions. The data of three experiments are averaged.

The heterogeneous property of *p*-TsOH@MMF was demonstrated by the reusability and leaching test. This heterogeneous property suggests that *p*-TsOH molecules should be stably immobilized in the MMF channel.

2-3-5. Deactivation of *p*-TsOH@MMF

A key feature of *p*-TsOH@MMF is non-covalent immobilization of *p*-TsOH molecules. This feature allows us to modify the catalytic activity by a simple method. The deactivation of *p*-TsOH@MMF was examined by simple soaking in acetonitrile to wash out the non-covalently immobilized *p*-TsOH molecules as below. The prepared *p*-TsOH@MMF was soaked in acetonitrile for 24 h at 20 °C, separated by decantation and washing with acetonitrile (*ca*. 5 mL, three times). The resulting crystals were then collected to obtain *p*-TsOH@MMF (washed) (Scheme 2-8). After each washing step, the number of *p*-TsOH molecules per a unit-space was estimated by a digestion NMR experiment.

Scheme 2-8. Schematic representation of the procedure for the preparation of *p*-TsOH@MMF (washed) and its deactivation test.

The double washing by acetonitrile reduced the number of *p*-TsOH molecules in the MMF channel from 1.6 to 0.76 per a unit-space. However, further decrease was not observed even after the third and fourth washing (Figure 2-10). This may be the result of slight decomposition of channel window which would

disturb the diffusion of molecules.

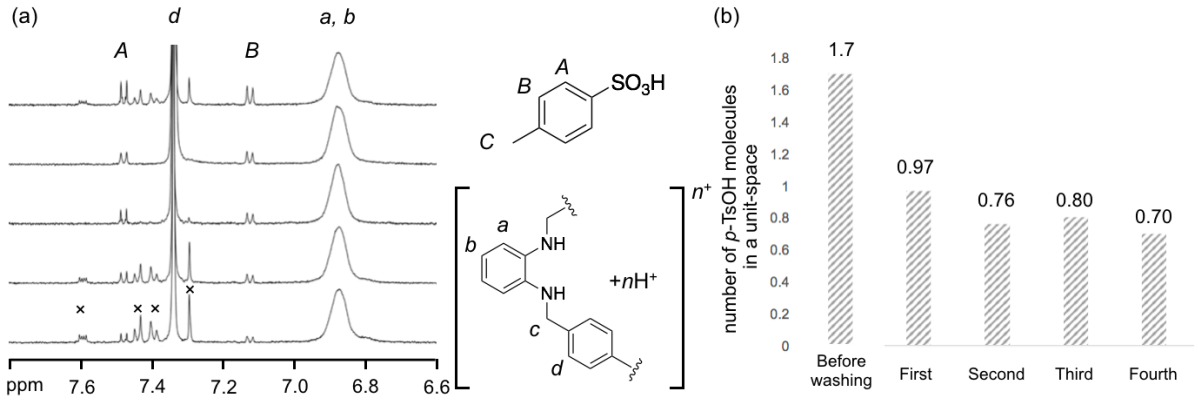

Figure 2-10. (a) ^{1}H NMR spectra of digestion NMR experiments after each washing step in acetonitrile (500 MHz, DCl/DMSO-d_6, 300 K). The spectra show those of each washing step: Before washing, and from first to fourth washing from the top. (b) The changes in the number of *p*-TsOH molecules in the MMF channel per a unit-space before washing and after each washing step (from the left to right).

After this preparation procedure, the resulting crystals *p*-TsOH@MMF (washed) were immediately used for the hydrolysis of **1**. The reaction did not proceed at all even after six weeks at 20 °C (Scheme 2-9), whereas the reaction with *p*-TsOH@MMF yielded 69% conversion after three weeks at 20 °C as described above. This result indicates the deactivation of *p*-TsOH@MMF. The reason why the remained *p*-TsOH molecules did not work can be explained by the slight decomposition of channel window, which would inhibit the diffusion of **1** to access the active *p*-TsOH sites in the MMF channel.

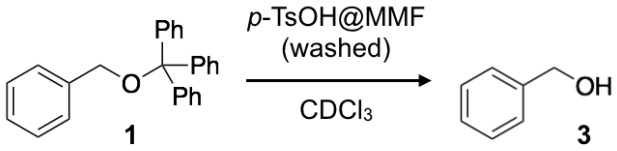

Entry	Condition	Conversion (%)
1	20 °C, 6 weeks	0

Scheme 2-9. Reaction with *p*-TsOH@MMF (washed). The data of three experiments are averaged. [**1**]: 2.0 mM. [H_2O]: 16 mM, *p*-TsOH@MMF (washed): 6 mol%. The number of equivalent of the catalyst was calculated based on the number of *p*-TsOH molecules immobilized in *p*-TsOH@MMF (washed).

2-3-6. Size-specific reaction

In the final step, size-specificity of the hydrolysis reaction using *p*-TsOH@MMF as a catalyst was examined. If the *p*-TsOH molecules were stably incorporated only in the MMF channel as expected, the size-specific reaction depending on the channel-size would be realized because the substrates larger than the channel window could not access the active *p*-TsOH site. Considering the channel-dimension of MMF (1.4 × 1.9 nm^2) and the kinetic diameters (d_{kin}) of the substrates, $PhCH_2OCPh_3$ **1** (d_{kin} = 1.1 nm) and Pd-$TPPCH_2OCPh_3$ **2** (d_{kin} = 1.7 nm) (TPP = tetraphenylporphyryl) were chosen to examine the size-specificity of the hydrolysis reaction using *p*-TsOH@MMF (Figure 2-11).

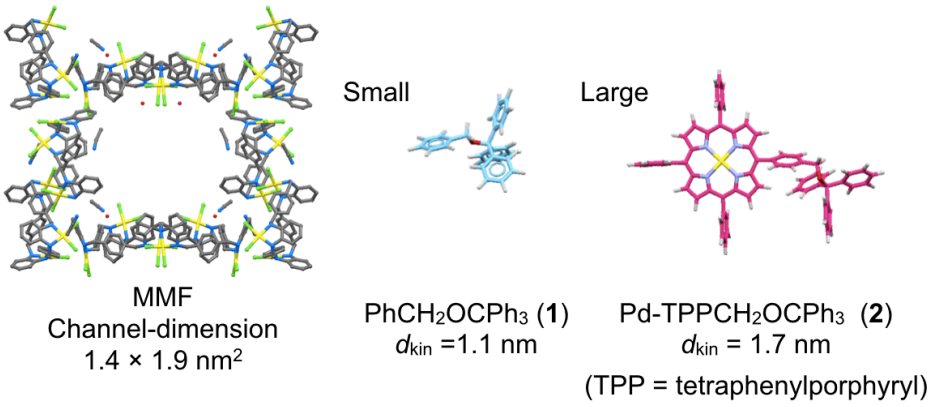

Figure 2-11. Channel-dimension of the MMF and kinetic diameters of the substrates. The kinetic diameters were briefly estimated by the molecular modeling.[9]

Whereas the hydrolysis reaction with the smaller $PhCH_2OCPh_3$ **1** gradually proceeded during three weeks and yielded 69% on average (Scheme. 2-10, entry 1), the larger Pd-$TPPCH_2OCPh_3$ **2** did not react at all even after three weeks (entry 3). The reproducibility of this reaction was confirmed by several independent experiments. On the other hand, homogeneous *p*-TsOH·H_2O hydrolyzed both substrates quantitatively in the same manner (Entries 2, 4), which excludes a concern about the difference in their reactivity between the two substrates. These results clearly suggest that the hydrolysis reaction with *p*-TsOH@MMF is size-specific, that is, only smaller substrates diffused into the channel can be catalyzed.

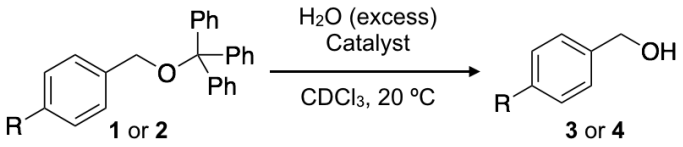

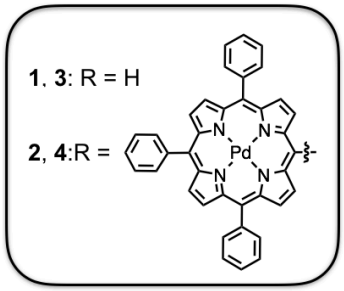

Entry	Reactant	Catalyst	Time	Conversion (%)
1[a]	**1**	*p*-TsOH@MMF (6 mol%)[b]	3 weeks	69
2		*p*-TsOH·H_2O (5 mol%)	1.5 h	96
3	**2**	*p*-TsOH@MMF (6 mol%)[b]	3 weeks	0
4		*p*-TsOH·H_2O (4 mol%)	1.5 h	94

Scheme 2-10. Comparison of hydrolysis reactions of the smaller **1** and the larger **2** by *p*-TsOH@MMF or homogeneous catalyst. [a] The data of three experiments are averaged. [b] The number of equivalent of the catalyst was calculated based on the number of *p*-TsOH molecules immobilized in *p*-TsOH@MMF. [**1**]: 2.2 mM, [**2**]: 2.1 mM. [H_2O]: 23 mM.

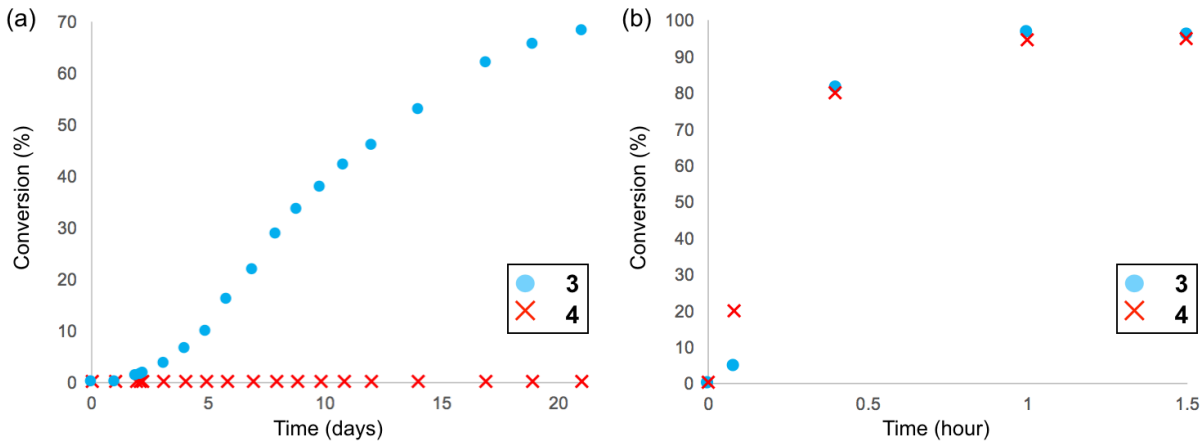

Figure 2-12. Time-course of the hydrolysis reaction of **1** and **2** using (a) *p*-TsOH@MMF (entries 1, 3) or (b) *p*-TsOH·H_2O (entries 2, 4) as a catalyst.

2-4. Conclusion

In this chapter, the stable non-covalent immobilization of an acid catalyst *p*-TsOH·H_2O in the MMF channel has been demonstrated. The *p*-TsOH@MMF catalyst showed the size-specific reactivity as well as typical properties as heterogeneous catalysts (Figure 2-13).

p-TsOH@MMF was easily prepared by soaking MMF crystals in an acetonitrile solution of *p*-TsOH·H_2O followed by successive washing in dichloromethane three times. The surface of the resulting crystals stably entrapped *ca*. 1.6 *p*-TsOH molecules per a unit-space. The crystallinity was almost retained, but the adsorption structure of *p*-TsOH molecules in *p*-TsOH@MMF could not be determined.

The catalytic activity of *p*-TsOH@MMF was examined by the hydrolysis reaction of tritylated substrates. The comparison with homogeneous systems, leaching and reusability tests, and the digestion NMR experiment after reaction clearly indicated a heterogeneous character of *p*-TsOH@MMF. Moreover, the easy modification of catalytic activity was achieved by simple washing in acetonitrile. Eventually, the size-specific reactivity was demonstrated through the reactions with different-sized substrates.

In this work, I have established a novel way to introduce catalytically active sites in the MMF nano-space and examined the catalytic activity of the resulting catalyst. The stable non-covalent immobilization of catalytic sites in a confined space of crystals enables to construct a reaction field for size-specific reaction in a heterogeneous catalyst. This approach would provide a variety of platforms for space-specific reactions in the MMF nano-space as seen in active sites of natural enzymes.

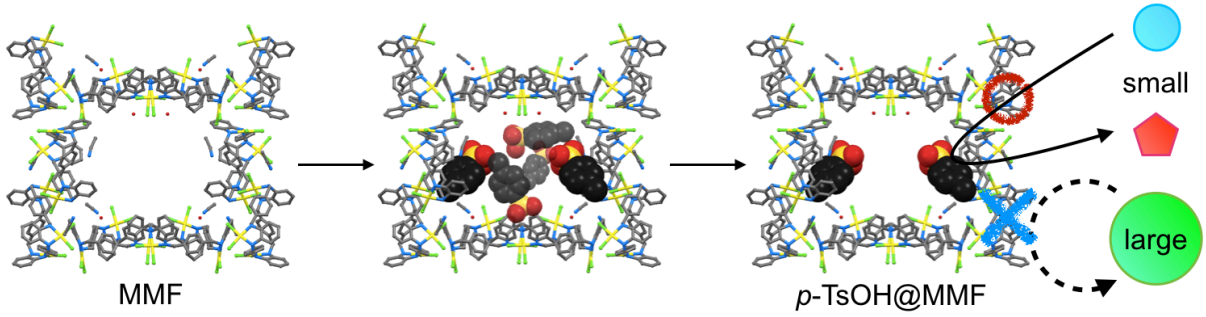

Figure 2-13. Stable immobilization of acid catalyst and its size-specific reactivity.

2-5. Experimental

Materials and methods

All chemicals are commercially available and were used without further purification otherwise noted. Column chromatography was performed using Merck Silica Gel 60 (230–400 mesh). MMF crystals were prepared according to our procedure previously reported after optimization.[10a] $PhCH_2OCPh_3$ **1** and Pd-$TPPCH_2OCPh_3$ **2** were synthesized according to the literatures.[12] NMR spectroscopic measurements were performed using a Bruker AVANCE 500 spectrometer (500 MHz for ^1H; 126 MHz for ^{13}C). NMR spectra were calibrated as below; $CDCl_3$: $Si(CH_3)_4$ = 0 ppm for ^1H, $CDCl_3$ = 77.16 ppm for ^{13}C. DMSO-d_6: $(CD_2H)CD_3SO$ = 2.50 ppm for ^1H. ESI-TOF mass spectra were recorded ona Waters LCT Premier XE spectrometers. Melting points were measured using a Yanaco MP-500D apparatus. IR spectra were recorded on a JASCO FT/IR-4200 spectrometer using ZnSe ATR method. Water contents were estimated by ^1H NMR analyses, and also confirmed by the result using a Mitsubishi CA-21 Karl-Fischer apparatus. Single-crystal X-ray crystallographic analysis was performed using a Rigaku RAXIS-RAPID imaging plate diffractometer with MoKα radiation or a Rigaku XtaLAB P200 system with CuKα radiation, and the obtained data were analyzed using a CrystalStructure crystallographic software package except for refinement, which was performed using a SHELXL-2013 program suite.[13] Solvent and guest molecules that are unbound to the molecular binding pockets are highly disordered in all crystal structures. Therefore, the contribution of electron density of their highly-disordered molecules was removed by the SQUEEZE function[14] except for the crystal structure of *p*-TsOH@MMF. Several restraints (bond distances, angles and thermal parameters) were applied to $[Pd_3\mathbf{L}Cl_6]$ and guest molecules in all crystal structures. Complexes $[Pd_3\mathbf{L}Cl_6]$ were refined anisotropically except for disordered parts. Solvent and guest molecules were refined isotropically. Hydrogen atoms were placed at the calculated positions and refined using a riding model. On the other hand, hydrogen atoms of water molecules could not be located in the difference electron density maps. High thermal factors of the guest and solvent molecules may be due to large thermal vibration arising from weak non-covalent interactions between the trapped molecules and the interior surface. The occupancies of guest molecules were refined based on electron densities using free variables in the SHELXL-2013 program, and the resulting moderate occupancies indicate that guest molecules are not entirely bound in each pocket and some pockets should be empty. X-ray structures were displayed using a Mercury program.

Preparation of MMF crystals

To a hot acetonitrile solution (68 mL) of macrocyclic hexamine **L** (12.6 mg, 20.0 μmol) was added a hot acetonitrile solution (3.1 mL) of $PdCl_2(CH_3CN)_2$ (*ca.* 16.3 mg, 3.1 eq.). The reaction mixture was well stirred on heating and filtered through membrane disc filter, and the filtrate was stood at room temperature for several weeks to afford MMF as yellow platelet crystals.

Syntheses of Pd-TPPCH$_2$OCPh$_3$ 2

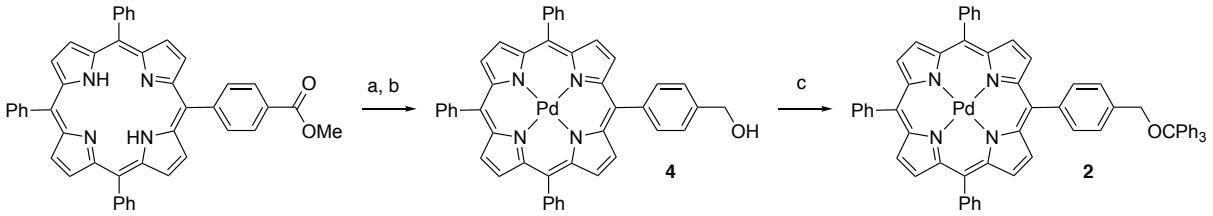

Scheme 2-11. Synthetic route for Pd-TPPCH$_2$OCPh$_3$ **2**. Reagents and conditions: (a) $LiAlH_4$, THF, rt, (b) $Pd(OAc)_2$, $CHCl_3$, reflux, (59% in 2 steps), (c) Ph_3CCl, Et_3N, CH_2Cl_2, rt (41%).

Synthesis of [5-(4-hydroxymethylphenyl)-10,15,20-triphenylporphyrinato] palladium(II) 4

To a stirred suspension of $LiAlH_4$ (18.8 mg, 0.495 mmol, 3.6 eq.) in dry THF (5 mL) was added dropwise a dry THF solution of 5-(4-carboxymethylphenyl)-10,15,20-triphenylporphyrin (92.6 mg, 0.138 mmol, 14 mL) at room temperature under an N_2 atmosphere. After stirring for 15 min at room temperature, water (100 mL) was carefully added to the reaction mixture. The separated aqueous layer was extracted with CH_2Cl_2 twice. The combined organic layer was dried over Na_2SO_4, filtered and concentrated. The residue was used for the next step without further purification.

To a stirred dry $CHCl_3$ solution of the residue (10 mL) was added $Pd(OAc)_2$ (61.1 mg, 0.272 mmol, 2.0 eq.) at room temperature under an N_2 atmosphere. After stirring for 68 h heating at reflux, water (40 ml) was added to the reaction mixture. The separated aqueous layer was extracted with $CHCl_3$ twice. The combined organic layer was dried over Na_2SO_4, filtered and concentrated to give a crude product (139 mg). The crude product was purified by silica-gel column chromatography (eluent: CH_2Cl_2) to afford **4** as a red solid (60.1 mg, 58.6% in 2 steps, 80.2 μmol).

^{1}H NMR (500 MHz; $CDCl_3$, 300 K): δ = 8.81-8.79 (m, 8H), 8.17-8.14 (m, 8H), 7.77-7.70 (m, 11H), 5.04 (d, J = 5.8 Hz, 2H), 1.95 (t, J = 5.9 Hz, 1H).

^{13}C NMR (126 MHz; $CDCl_3$, 300 K): δ = 141.92, 141.75, 141.73, 141.70, 141.32, 140.45, 134.44, 134.25, 131.18, 131.06, 127.92, 126.87, 125.49, 121.95, 121.92, 121.52, 65.56.

* 7 peaks are overlapped in ^{13}C NMR.

IR (ATR): υ = 3050.8, 2918.7, 2852.2, 1597.7, 1540.9, 1440.6, 1352.8, 1236.2, 1086.7, 1013.4.

HRMS (EST-TOF): *m/z* calcd for $[C_{45}H_{30}N_4OPd]^{\bullet+}$ 748.1471; found: 748.1489.

Mp.: > 300 °C.

Synthesis of [5-(4-triphenylmethoxymethylphenyl)-10,15,20-triphenylporphyrinato]palladium(II) 2

To a stirred dry CH_2Cl_2 solution of [5-(4-hydroxymethyl-phenyl)-10,15,20-triphenylporphyrinato] palladium(II) **4** (60.1 mg, 80.2 μmol, 6.0 mL) were added trityl chloride (23.4 mg, 83.9 μmol, 1.1 eq.) and triethylamine (35 μL, 0.25 mmol, 3.1 eq.) at room temperature under an N_2 atmosphere. After stirring for 20 h at reflux temperature, trityl chloride (20.0 mg, 71.7 μmol, 0.90 eq.) and triethylamine (35 μL, 0.25 mmol, 3.1 eq.) were added again to the mixture at room temperature. After stirring for another 8 h at reflux temperature, saturated aqueous ammonium chloride was added to the reaction mixture. The separated aqueous layer was extracted with CH_2Cl_2 twice. The combined organic layer was dried over Na_2SO_4, filtered and concentrated to give a crude product (124 mg). The crude product was purified by silica-gel column chromatography (eluent: CH_2Cl_2) and reprecipitation (CH_2Cl_2-CH_3OH) to afford **2** as a red-purple solid (32.7 mg, 41.1%, 33.0 μmol).

^{1}H NMR (500 MHz; $CDCl_3$, 300 K): δ = 8.84 (d, J = 4.9 Hz, 2H), 8.81 (d, J = 5.0 Hz, 2H), 8.80 (s, 4H), 8.17 (dt, J = 7.8, 1.4 Hz, 6H), 8.12 (d, J = 8.0 Hz, 2H), 7.76-7.71 (m, 11H), 7.68 (dt, J = 8.4, 1.6 Hz, 6H) 7.41 (t, J = 7.7 Hz, 6H), 7.32 (tt, J = 7.3, 1.4 Hz, 3H), 4.56 (s, 2H).

^{13}C NMR (126 MHz; $CDCl_3$, 300 K): δ = 144.36, 141.96, 141.82, 141.74, 141.72, 140.63, 138.88, 134.27, 134.18, 131.25, 131.13, 131.12, 129.03, 128.15, 127.90, 127.32, 126.86, 125.35, 121.88, 121.86, 87.47, 65.99.

* 7 peaks are overlapped in ^{13}C NMR.

IR (ATR): υ = 3054.7, 3024.8, 2922.6, 2851.2, 1953.5, 1809.9, 1597.7, 1490.7, 1447.3, 1352.8, 1311.4, 1074.2, 1013.4.

HRMS (ESI-TOF): *m/z* calcd for $[C_{64}H_{44}N_4OPd]^{\bullet+}$ 990.2571; found: 990.2612.

Mp.: 250 °C (decomp.).

Preparation and characterization of *p*-TsOH@MMF

Time-course analysis of encapsulation behavior

MMF crystals were soaked in an acetonitrile solution of *p*-TsOH·H_2O (0.80 M) at room temperature for a fixed time. The resulting crystals were collected by filtration, washed with a small amount of CH_3CN (*ca.* 200 μL) and air-dried for ten seconds on a filter paper. The crystals were subjected to digestion NMR experiments to estimate the number of *p*-TsOH molecules encapsulated in a unit-space of MMF.

Single-crystal XRD analysis of MMF including *p*-TsOH molecules

MMF crystals were soaked in an acetonitrile solution of *p*-TsOH·H_2O (0.80 M) at room temperature for a given time. One of the resulting crystals was picked up and covered with fluorolube then rapidly cooled to –180 °C under cold N_2 flow on a goniometer to subject to a single-crystal X-ray diffraction measurement. Even after 1 h soaking, the adsorption of *p*-TsOH molecules appeared saturated (1 h: 46%, 1 day: 49% for the occupancy).

Crystal data of MMF including *p*-TsOH molecules (0.80 M, 1 h soaking)

Crystal data for $(Pd_3\mathbf{L}Cl_6)_2\cdot(C_7H_8SO_3)_{0.46}\cdot(C_2H_3N)_{2.81}\cdot(H_2O)_5$: $C_{92.84}H_{106.11}Cl_{12}N_{14.81}O_{6.38}Pd_6S_{0.46}$, F_w = 2610.15, crystal dimensions 0.39 × 0.24 × 0.07 mm^3, monoclinic, space group $P2_1/c$, a = 19.5719(3), b = 52.1873(10), c = 14.3568(2) Å, β = 90.6995 (13)°, V = 14663.0(4) Å^3, Z = 4, ρ_{calcd} = 1.182 g cm^{-3}, μ = 82.121 cm^{-1}, T = 93 K, λ (CuKα) = 1.54187 Å , $2\theta_{max}$ = 147.2°, 61323/28280 reflections collected/unique (R_{int} = 0.0448), R_1 = 0.0997 ($I > 2\sigma(I)$), wR_2 = 0.2677 (for all data), GOF = 1.033, largest diff. peak and hole 2.27 /–2.26 eÅ^{-3}. The contribution of the electron density in the void was removed by the SQUEESE function.

Crystal data of MMF including *p*-TsOH molecules (0.80 M, 1 day soaking)

Crystal data for $(Pd_3\mathbf{L}Cl_6)_2\cdot(C_7H_8SO_3)_{0.49}\cdot(C_2H_3N)_{2.48}\cdot(H_2O)_4$: $C_{92.37}H_{103.33}Cl_{12}N_{14.48}O_{5.46}Pd_6S_{0.49}$, F_w = 2583.32, crystal dimensions 0.35 × 0.22 × 0.06 mm^3, monoclinic, space group $P2_1/c$, a = 19.5739(3), b = 52.2519(11), c = 14.3559(2) Å, β = 90.7164 (11)°, V = 14681.7(4) Å^3, Z = 4, ρ_{calcd} = 1.169 g cm^{-3}, μ = 81.953 cm^{-1}, T = 93 K, λ (CuKα) = 1.54187 Å , $2\theta_{max}$ = 147.2°, 66190/28359 reflections collected/unique (R_{int} = 0.0508), R_1 = 0.1092 ($I > 2\sigma(I)$), wR_2 = 0.2747 (for all data), GOF = 1.030, largest diff. peak and hole 2.88 /–2.39 eÅ^{-3}. The contribution of the electron density in the void was removed by the SQUEESE function.

Screening of washing solvents

Established encapsulation procedure was used to prepare MMF crystals including *ca.* 5 *p*-TsOH molecules as below. MMF crystals were soaked in an acetonitrile solution of *p*-TsOH·H_2O (0.75 M) for 20 h at 20 °C. The resulting crystals were collected by filtration, washed with a small amount of CH_3CN (*ca*. 200 μL) and air-dried for ten seconds on a filter paper to afford MMF crystals including *ca.* 5 *p*-TsOH molecules.

The resulting crystals were soaked in each solvent (acetonitrile, dichloromethane or *n*-hexane) for 12 h at 20 °C, and then were collected by filtration, washed with a small amount of the solvent (*ca*. 200 μL) and air-dried for ten seconds on a filter paper. This washing operation was repeated three times in total.

After each step, the number of *p*-TsOH per a unit-space was estimated by digestion NMR experiments.

Optimization of washing procedure with dichloromethane

Established encapsulation procedure was used as below. MMF crystals were soaked in an acetonitrile solution of *p*-TsOH·H_2O (0.75 M, MMF/acetonitrile = 10 mg/mL) for 20 h at 20 °C. The resulting crystals were collected by filtration, washed with a small amount of acetonitrile (*ca*. 200 μL) and air-dried for ten seconds on a filter paper to afford MMF crystals including 5.2 ± 0.5 *p*-TsOH molecules.

The resulting crystals were soaked in dichloromethane (MMF/dichloromethane = 1 mg/mL) for one day at 20 °C, and then were collected by decantation. This washing operation was repeated four times in total.

After each step, the number of *p*-TsOH per a unit-space was estimated by digestion NMR experiments. In each measurement, three batches of NMR samples were analyzed to average the numbers with the standard deviation.

Preparation of *p*-TsOH@MMF

The established encapsulation procedure was used as below. MMF crystals were soaked in an acetonitrile solution of *p*-TsOH·H_2O (0.75 M, MMF/acetonitrile = 10 mg/mL) for 20 h at 20 °C. The resulting crystals were collected by filtration, washed with a small amount of CH_3CN (*ca*. 200 μL) and air-dried for ten seconds on a filter paper to afford MMF crystals including 5.2 ± 0.5 *p*-TsOH molecules.

The resulting crystals were soaked in dichloromethane (MMF/ dichloromethane = 1 mg/mL) for one day at 20 °C, and then were collected by decantation. This washing operation was repeated three times in total to afford *p*-TsOH@MMF. The number of *p*-TsOH per a unit-space of *p*-TsOH@MMF was estimated by

digestion NMR experiments. After the preparation, this catalyst was immediately used for catalytic reactions.

Characterization of *p*-TsOH@MMF

The chemical composition of *p*-TsOH@MMF except for water was estimated to be $(Pd_3\mathbf{L}Cl_6)_4\cdot(p\text{-}TsOH)_{1.6}\cdot(CHCl_3)_8\cdot(H_2O)_n$ based on the integral ratios in the ^{1}H NMR spectrum. The presence of water in *p*-TsOH@MMF was suggested by the crystal structure. The number of water molecules included in *p*-TsOH@MMF was temporarily assumed to be $n = 20$ ($Mw = 6224.8$). Because the number of water molecules included in as-synthesized MMF crystals was estimated to be 36 by previous elemental analysis ($(Pd_3\mathbf{L}Cl_6)_4\cdot(CH_3CN)_2\cdot(H_2O)_{36}$),[10a] the number n and the molecular weight Mw of *p*-TsOH@MMF should fall within $0 \leqq n \leqq 36$ and $5864.5 \leqq Mw \leqq 6513.0$, respectively. Therefore, the error of catalyst quantity used here ($n = 20$, $Mw = 6224.8$) falls within 10% regardless of water contents.

Single-crystal XRD analysis of *p*-TsOH@MMF

MMF crystals were soaked in an acetonitrile solution of *p*-TsOH·H_2O (0.75 M) for 20 h at 20 °C, collected by decantation. To wash out the excess amount of *p*-TsOH·H_2O, the crystals were soaked in CH_2Cl_2 for 24 h at 20 °C. After soaking, the solvent was removed by decantation and replaced with pure CH_2Cl_2. This washing operation was repeated three times in total. After that, a crystal was picked up and mixed with fluorolube then rapidly cooled to –180 °C under cold N_2 flow on a goniometer to subject to a single-crystal X-ray diffraction measurement.

Crystal data for $(Pd_3\mathbf{L}Cl_6)_2\cdot(CH_2Cl_2)_2\cdot(H_2O)_8$: $C_{86}H_{104}Cl_{116}N_{12}O_8Pd_6$, $F_w = 2639.49$, crystal dimensions 0.29 × 0.23 × 0.07 mm^3, monoclinic, space group $P2_1/c$, $a = 19.5796(13)$, $b = 52.142(3)$, $c = 14.2469(10)$ Å, $\beta = 91.162(2)°$, $V = 14542.0(16)$ Å^3, $Z = 4$, $\rho_{calcd} = 1.206$ g cm^{-3}, $\mu = 10.607$ cm^{-1}, $T = 93$ K, λ (MoKα) = 0.71075 Å , $2\theta_{max} = 34.0°$, 35169/7998 reflections collected/unique ($R_{int} = 0.1001$), $R_1 = 0.1612$ ($I > 2\sigma(I)$), $wR_2 = 0.4455$ (for all data), GOF = 1.124, largest diff. peak and hole 1.20/–0.78 eÅ^{-3}.

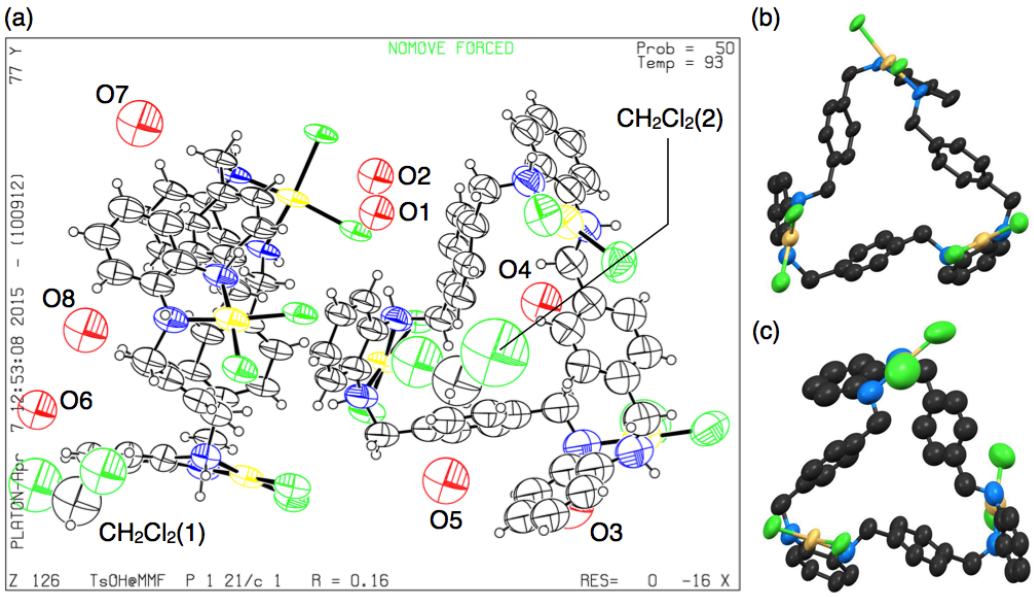

Figure 2-14. (a) ORTEP drawing of the asymmetric unit of *p*-TsOH@MMF (50% probability level). Ellipsoid model (50% probability level) of (b) (*P*)-*syn*- and (c) (*M*)-*anti*-[Pd_3**L**Cl_6]. Hydrogen atoms are omitted for clarity. C: black, N: blue, Pd: yellow, Cl: green and O: red.

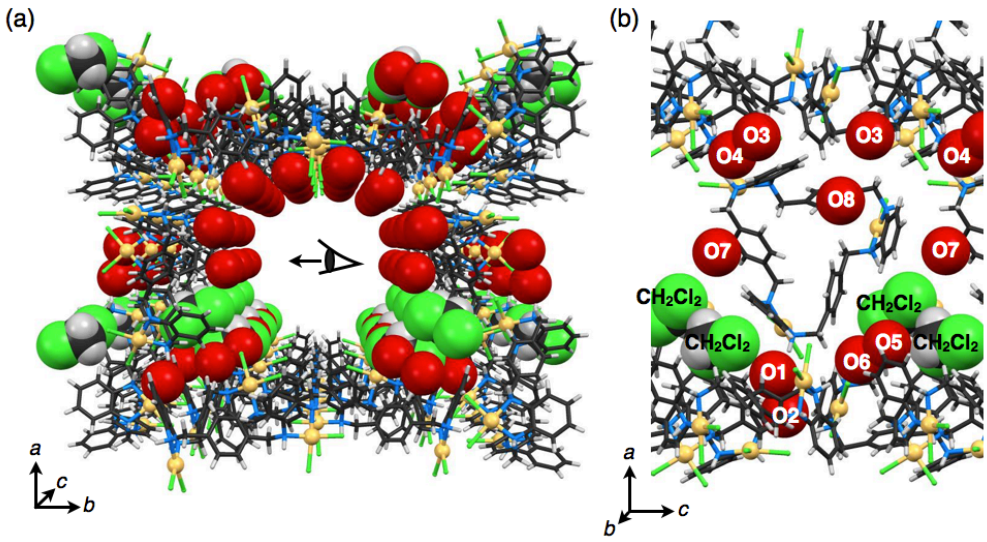

Figure 2-15. Crystal structures of TsOH@MMF (MMF: stick model, solvent: space-filling model). (a) Single nano-channel. (b) Side surface of the nano-channel. C: black, N: blue, Pd: yellow, Cl: green and O: red.

Hydrolysis reactions of trityl group with *p*-TsOH@MMF

General remarks

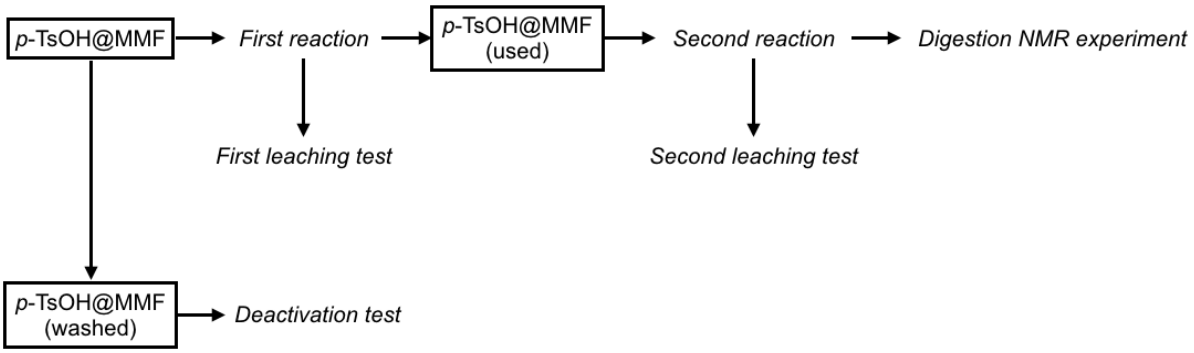

Scheme 2-12. Schematic representation of the outline of general procedures for catalytic reactions

In this section, we used fresh crystals of *p*-TsOH@MMF collected from the same synthetic batch. Most reactions were conducted in three independent batches to confirm the reproducibility. Mole number of the catalyst was calculated based on that of *p*-TsOH included in *p*-TsOH@MMF. $CDCl_3$ was filtered through an oven-dried alumina (activated basic) column to remove trace amount of acids in prior to use. A small amount of 1,1,2,2-tetrachloroethane was added as an internal standard (2.0 mM) to estimate the concentrations of substrates, products and water in ^{1}H NMR analyses. The $CDCl_3$ solution prepared as above was soon used as reaction solvent. The amount of water in a $CDCl_3$ solution was estimated from the signal intensity of water in ^{1}H NMR analysis, whose results were comparable to water contents measured by Karl-Fischer method. The reaction conversions were estimated by the comparison of the integral ratio of the product and internal standard. Note that the term "0% yield" means that we could not detect the products at all in ^{1}H NMR analyses.

Size-specific reaction (deprotection of 1 or 2)

Reaction with $PhCH_2OCPh_3$ 1

In order to confirm the reproducibility of this reaction, independent three samples were prepared as below. To freshly-prepared *p*-TsOH@MMF (0.39, 0.32, and 0.31 mg, 0.094, 0.077, and 0.075 μmol as *p*-TsOH, respectively) were added $CDCl_3$ solutions of $PhCH_2OCPh_3$ (**1**) (2.2 mM, 0.78, 0.64, and 0.62 mL, 1.7, 1.4, and 1.4 μmol, respectively). The mixtures were transferred into NMR tubes and stood at 20 °C to pursue the reaction time-course by ^{1}H NMR measurements. The water contents in the initial states were

estimated to be 23 mM by ^{1}H NMR analyses.

Reaction with Pd-TPPCH$_2$OCPh$_3$ 2

To freshly-prepared *p*-TsOH@MMF (0.39 mg, 0.094 μmol as *p*-TsOH) was added a $CDCl_3$ solution of Pd-TPPCH$_2$OCPh$_3$ **2** (2.1 mM, 0.78 mL, 1.6 μmol). Then, the mixture was transferred into an NMR tube and stood at 20 °C to pursue this reaction time-course by ^{1}H NMR measurements. As a result, no reaction proceeded even after three weeks. The water content in the initial state was estimated to be 23 mM by ^{1}H NMR analyses.

Control experiments

Homogeneous deprotection of 1 with *p*-TsOH·H$_2$O

A $CDCl_3$ solution of PhCH$_2$OCPh$_3$ **1** (3.0 mM, 0.40 mL, 1.2 μmol) was evaporated in an NMR tube. To this was added a $CDCl_3$ solution of *p*-TsOH·H$_2$O (0.10 mM, 0.60 mL, 0.060 μmol, 5 mol%). The mixture was stood at 20 °C to pursue the reaction time course by ^{1}H NMR measurements. As a result, deprotection reaction of **1** yielded 96% conversion in 1.5 h. The water content in the initial state was estimated to be 20 mM by ^{1}H NMR analyses.

Control reaction with as-synthesized MMF crystals

To freshly-prepared MMF crystals (1.27 mg, 0.273 μmol as the unit-space of MMF, 20 mol%) was added a $CDCl_3$ solution of PhCH$_2$OCPh$_3$ **1** (1.9 mM, 0.70 mL, 1.3 μmol). Then, the mixture was transferred into an NMR tube and stood at 20 °C to pursue the reaction time-course by ^{1}H NMR measurements. As a result, no reaction proceeded even after three weeks. Note that in the cases of the deprotection of **1** with *p*-TsOH@MMF (6 mol% for *p*-TsOH), the amount of the unit-space was corresponding to 4 mol%. The water content of the initial state was estimated to be 29 mM by ^{1}H NMR analyses.

Comparison of acid lability between 1 and 2

To $CDCl_3$ solutions of PhCH$_2$OCPh$_3$ **1** (2.0 mM, 0.60 mL, 1.2 μmol) and Pd-TPPCH$_2$OCPh$_3$ **2** (2.0 mM, 0.60 mL, 1.2 μmol), $CDCl_3$ suspensions of *p*-TsOH·H$_2$O (50 μL; 0.06 μmol for **1**, 0.05 μmol for **2**) were added. The mixtures were stood at 20 °C to pursue the reaction time-course by ^{1}H NMR measurements. As a result, both substrates **1** and **2** showed almost same reactivity (96, 94% conversion after 1.5 h, respectively).

In addition, dissociation of metal ions of **2** and **4** was not detected under these conditions. The water contents in the initial states were estimated to be 27 and 35 mM, respectively, by ^{1}H NMR measurements.

Guest uptake of 1 into MMF nano-space

MMF crystals were soaked in a $CDCl_3$ solution of $PhCH_2OCPh_3$ **1** (0.5, 0.1, 0.01 M) for one day at 20 °C. The MMF crystals were collected by filtration, washed with a small amount of $CDCl_3$ (*ca*. 200 μL) and air-dried for ten seconds on a filter paper. The number of **1** encapsulated in a unit-space of MMF was estimated by digestion NMR experiments. In the case of [**1**] = 0.5 M (Scheme 2-13, entry 1), 0.20 molecules of **1** were observed per a unit-space of MMF.

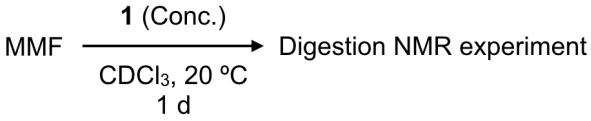

Entry	Conc.	Result
1	0.50 M	0.20 molecules / unit-space
2	0.10 M	not detected
3	0.010 M	not detected

Scheme 2-13. Digestion experiments for MMF crystals soaked in $CDCl_3$ solutions of **1**.

Demonstration of heterogeneous character of *p*-TsOH@MMF

Leaching tests with supernatants of the first reactions

After the first reactions, the reaction mixtures were decanted to collect their supernatants. Then the supernatants containing both **1** and **3** were filtered with cotton. To the filtrates were added $CDCl_3$ solutions of $PhCH_2OCPh_3$ **1** (6.7 mM, 0.23, 0.19, and 0.19 mL, 1.5, 1.3, and 1.3 μmol: entry 1-3, respectively) and these mixtures were messed up to 0.78, 0.64, and 0.62 mL with $CDCl_3$, respectively. The mixtures were stood at 20 °C to pursue the reaction time-course by ^{1}H NMR measurements. Because the ratios of **1** and **3** did not change at all even after three weeks, reaction temperature was raised to 50 °C and stood another three weeks to pursue the reactions by ^{1}H NMR measurements. No further conversion of **1** proceeded even after three weeks at 50 °C. The water contents of entry 1–3 in initial states were estimated to be 25 mM by ^{1}H NMR analyses.

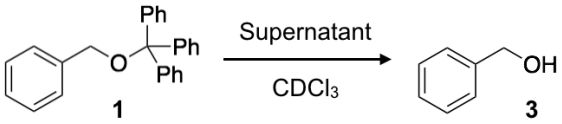

Entry	Condition	Conversion (%)
1	20 °C, 3 weeks	< 1
	+ 50 °C, 3 weeks	< 1
2	20 °C, 3 weeks	< 1
	+ 50 °C, 3 weeks	< 1
3	20 °C, 3 weeks	< 1
	+ 50 °C, 3 weeks	< 1

Scheme 2-14. Leaching tests with supernatants of the first reactions ($CDCl_3$, 20 °C to 50 °C). [H_2O]: 25 mM.

Reusability of *p*-TsOH@MMF

After the first reactions, the reaction mixtures were decanted to remove supernatants. To the remained crystals was added pure $CDCl_3$ (*ca*. 100 μL) and the supernatants were removed by careful decantation after five minutes. This washing operation was repeated again. Then the supernatants were removed by careful decantation to afford *p*-TsOH@MMF (used). After the preparation, these catalysts were immediately used for second reaction.

To freshly-prepared *p*-TsOH@MMF (reused) (if there was no loss of crystals during preparation of *p*-TsOH@MMF (reused); 0.39, 0.32. and 0.31 mg, 0.094, 0.077, and 0.075 μmol as *p*-TsOH: entries 1, 2, and 3, respectively) were added a $CDCl_3$ solutions of $PhCH_2OCPh_3$ **1** (2.0 mM, 0.78, 0.64, and 0.62 mL, 1.6, 1.3, and 1.2 μmol: entries 1, 2, and 3, respectively). The mixtures were stood at 20 °C to pursue the reactions by ^{1}H NMR measurements. Because the reaction did not proceed at all even after three weeks, temperature was raised to 50 °C and the mixtures were stood another several weeks to pursue the reactions by ^{1}H NMR measurements. As a result, deprotection of **1** proceeded to yield 60% on average (24%, 65%, and 91%, respectively) after three weeks. The water contents of entry 1–3 in initial states were estimated to be 12 mM by ^{1}H NMR analyses.

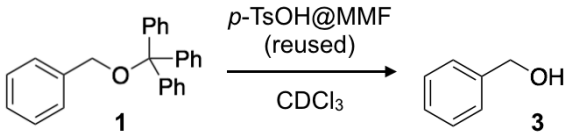

Entry	Condition	Conversion (%)
1	20 °C, 3 weeks	0
	+ 50 °C, 3 weeks	24
2	20 °C, 3 weeks	0
	+ 50 °C, 3 weeks	65
3	20 °C, 3 weeks	0
	+ 50 °C, 3 weeks	91

Scheme 2-15. Second reaction with *p*-TsOH@MMF (used) (6 mol%) in $CDCl_3$ at 20 °C or 50 °C. [H_2O]: 12 mM.

Second leaching tests with supernatants of the second reactions

After the second reactions, the reaction mixtures were decanted to collect their supernatants. Then the supernatants containing both **1** and **3** were filtered with cotton. To the filtrates were added $PhCH_2OCPh_3$ **1** (0.51, 0.43, and 0.41 mg, 1.5, 1.2, and 1.2 μmol: entries 1-3, respectively) and these mixtures were messed up to 0.78, 0.64, and 0.62 mL with $CDCl_3$, respectively. The mixtures were stood at 50 °C to pursue the reaction time-course by ^{1}H NMR measurements. As a result, no further conversion of **1** proceeded even after three weeks. The water contents of entries 1–3 in the initial states were estimated to be 25 mM by ^{1}H NMR analyses.

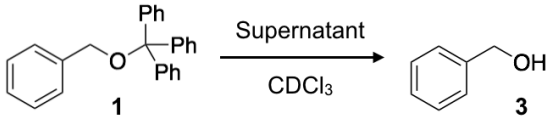

Entry	Condition	Conversion (%)
1	50 °C, 3 weeks	< 1
2	50 °C, 3 weeks	< 1
3	50 °C, 3 weeks	< 1

Scheme 2-16. Second leaching test with supernatants of the second reactions ($CDCl_3$, 50 °C). [H_2O]: 25 mM.

Digestion NMR experiments of *p*-TsOH@MMF after the second reactions

After the second reactions, the reaction mixtures were decanted to remove supernatants. To the remained crystals was added pure $CDCl_3$ (*ca*. 100 μL) and the mixtures were stood for five minutes and then decanted to remove supernatants. This washing operation was repeated once more. The resulting crystals

were dried up in vacuo to subject to digest NMR experiments. Most of *p*-TsOH molecules encapsulated in the initial *p*-TsOH@MMF crystals (1.6 ± 0.2 molecules/unit-space) were remained in the crystals even after the second reactions (1.4 ± 0.2 molecules/unit-space).

Deactivation of *p*-TsOH@MMF by acetonitrile washing

Preparation of *p*-TsOH@MMF (washed)

As-prepared *p*-TsOH@MMF crystals were soaked in acetonitrile (MMF/acetonitrile = 1 mg/mL) for one day at 20 °C, separated by decantation and washed with acetonitrile (*ca*. 5 mL). This washing operation was further repeated three times. After that, the resulting crystals were collected by filtration, washed with a small amount of acetonitrile and air-dried for ten seconds on a filter paper to afford *p*-TsOH@MMF (washed). After each washing step, the amount of *p*-TsOH·H_2O remained in the unit-space was estimated by digestion NMR experiments. After the preparation, this catalyst was immediately used for deprotection reactions.

Reaction with *p*-TsOH@MMF (washed)

To *p*-TsOH@MMF (washed) freshly prepared (0.82, 0.72, and 0.70 mg, 0.092, 0.081, and 0.079 μmol as *p*-TsOH: entries 1-3, respectively) were added $CDCl_3$ solutions of $PhCH_2OCPh_3$ **1** (2.0 mM, 0.82, 0.72, and 0.70 mL, 1.6, 1.4, and 1.4 μmol: entries 1-3, respectively). The mixtures were stood at 20 °C to pursue the reaction time-course by ^1H NMR measurements. No reaction proceeded even after six weeks. The water contents of entries 1–3 in the initial states were estimated to be 15 mM by ^1H NMR analyses.

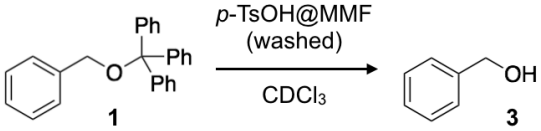

Entry	Condition	Conversion (%)
1	20 °C, 6 weeks	0
2	20 °C, 6 weeks	0
3	20 °C, 6 weeks	0

Scheme 2-17. Deactivation tests with *p*-TsOH@MMF (washed) (6 mol%) in $CDCl_3$ at 20 °C. [**1**]: 2.0 mM. [H_2O]: 15 mM.

2-6. References

[1] (a) G. Erti, H. Knözinger, J. Weitkamp Eds., *Handbook of Heterogeneous Catalysis*, WILEY-VCH Verlag GmbH & Co. KGaA: Weinheim, **1997**. (b) J. Li, A. Corma, J. Yu, *Chem. Soc. Rev.* **2015**, *44*, 7112-7127.

[2] (a) C. T. Kresge, M. E. Leonowicz, W. J. Roth, J. C. Vartuli, J. S. Beck, *Nature* **1992**, *359*, 710-712. (b) A. K. Cheetham, G. Férey, T. Loiseau, *Angew. Chem. Int. Ed.* **1999**, *38*, 3268-3292. (c) Z. A. ALOthman, *Materials* **2012**, *5*, 2874-2902. (d) C. T. Kresge, W. J. Roth, *Chem. Soc. Rev.* **2013**, *42*, 3663-3670.

[3] (a) S. Kitagawa, R. Kitaura, S. Noro, *Angew. Chem. Int. Ed.* **2004**, *43*, 2334-2375. (b) S. Kitagawa, R. Matsuda, *Coord. Chem. Rev.* **2007**, *251*. 2490-2509.

[4] (a) M. E. Davis, *Nature* **2002**, *417*, 813-821. (b) X. Feng, X. Ding, D. Jiang, *Chem. Soc. Rev.* **2012**, *41*, 6010-6022.

[5] (a) A. Clearfield, *Chem. Rev.* **1988**, *88*, 125-148. (b) T. Linssen, K. Cassiers, P. Cool, E. F. Vansant, *Adv. Coll. Int. Sci.* **2003**, *103*, 121-147. (c) E. A. Pidko, E. J. M. Hensen, R. A. van Santen, *Proc. R. Soc. A* **2012**, *468*, 2070-2086. (d) K. K. Tanabe, S. M. Cohen, *Chem. Soc. Rev.* **2011**, *40*, 498-511. (e) P. Deria, J. E. Mondloch, O. Karagiaridi, W. Bury, J. T. Hupp, O. K. Farha, *Chem. Soc. Rev.* **2014**, *43*, 5896-5912. (f) S. M. Cohen, *J. Am. Chem. Soc.* **2017**, *139*, 2855-2863.

[6] (a) T. Maschemeyer, F. Rey, G. Sankar, J. M. Thomas, *Nature* **1995**, *378*, 159-162. (b) A. Sinnema, R. J. J. Jansen, K. Pamin, H. van Bekkum, *Catal. Lett.* **1995**, *30*, 241-252.

[7] (a) V. R. Choudhary, A. K. Kinage, C. Sivadinarayana, M. Guisnet, *J. Catal.* **1996**, *158*, 23-33. (b) V. R. Choudhary, S. K. Jana, B. P. Kiran, *Catal. Lett.* **1999**, *59*, 217-219. (c) B. M. Abu-Zied, W. Schwieger, A. Unger, *Appl. Catal. B* **2008**, *84*, 277-288.

[8] (a) Y.-H. Kiang, G. B. Gardner, S. Lee, Z. Xu, E. B. Lobkovsky, *J. Am. Chem. Soc.* **1999**, *121*, 8204-8215. (b) M. J. Ingleson, J. P. Barrio, J. B. Guilbaud, Y. Z. Khimyak, M. J. Rosseinsky, *Chem. Commun.* **2008**, 2680-2682.

[9] (a) S. Tashiro, M. Shionoya, *Bull. Chem. Soc. Jpn.* **2014**, *87*, 643-654. (b) H. Zhang, R. Zou, Y. Zhao, *Coord. Chem. Rev.* **2015**, *292*, 74-90.

[10] (a) S. Tashiro, R. Kubota and M. Shionoya, *J. Am. Chem. Soc.* **2012**, *134*, 2461-2464. (b) R. Kubota, S. Tashiro, T. Umeki, M. Shionoya, *Supramol. Chem.* **2012**, *24*, 867-877. (c) S. Tashiro, T. Umeki, R. Kubota, M. Shionoya, *Angew. Chem. Int. Ed.* **2014**, *136*, 17946-17949. (d) R. Kubota, S. Tashiro, M. Shiro, M. Shionoya, *Nat. Chem.* **2014**, *6*, 913-918.

[11] T. C. Keller, S. Isabettini, D. Verboekend, E. G. Rodrigues and J. Pérez-Ramírez, *Chem. Sci.* **2014**, ***5***, 677–684.

[12] (a) J. P. Hill, A. S. D. Sandanayaka, A. L. McCarty, P. A. Karr, M. E. Zandler, R. Charvet, K. Ariga, Y. Araki, O. Ito, F. D'Souza, *Eur. J. Org. Chem.* **2006**, 595-603. (b) M. Maltese, M. C. Vergari and M. P. Donzello, *Tetrahedron Lett.* **2011**, *52*, 483-487.

[13] G. M. Sheldrick, SHELXL-97, *Program for refinement of crystal structure* (University of Göttingen, Germany, 1997); G. M. Sheldrick, SHELXL-2013 (University of Göttingen, Germany, 2013).

[14] A. L. Spek, *PLATON, A Multipurpose Crystallographic Tool* (Utrecht University, The Netherlands, 2001).

第三章については、５年以内に雑誌等で刊行予定のため、非公開。

第四章については、５年以内に雑誌等で刊行予定のため、非公開。

第五章については、５年以内に雑誌等で刊行予定の内容を含むため、非公開。

A list of publications

[1] "Non-Covalent Immobilisation of *p*-Toluenesulfonic Acid in a Porous Molecular Crystal for Size-Specific Acid-Catalysed Reactions", Shohei Tashiro, Hirotaka Yonezawa, Ryou Kubota, Tsutomu Umeki, and Mitsuhiko Shionoya, *Chem. Commun.* **2016**, *52*, 7657-7660.

Acknowledgement

This research was promoted under the supervision of Prof. Dr. Mitsuhiko Shionoya (The University of Tokyo). I greatly appreciate him for the impressive discussions and warmest support for my laboratory life.

I am deeply grateful to associate Prof. Dr. Shohei Tashiro (The University of Tokyo) for his honest aid from research to daily life. I appreciate assistant Prof. Dr. Hitoshi Ube and assistant Prof. Dr. Yusuke Takezawa (The University of Tokyo) for their smart ideas and concrete advices.

I feel thank to all member of Shionoya laboratory for the support of daily life in the laboratory. In particular, I would like to say a lot of thanks to Mr. Ryo Yamada and Ms. Qian Zhang for the friendly rival relationship to encourage our researches each other.

I sincerely appreciate Prof. Dr. Masahiro Ehara (The Institute for Molecular Science) and Mr. Takafumi Shiraogawa (SOKENDAI) for the collaboration works from the view point of theoretical calculations.

I am strongly grateful to Prof. Dr. Takeaki Ozawa and assistant Prof. Dr. Rintaro Shimada (The University of Tokyo) for the collaboration work including Raman spectroscopy.

I appreciate Prof. Dr. Eiichi Nakamura, associate Prof. Dr. Koji Harano, associate Prof. Ilies Laurean, Mr. Hiroki Nishioka, and Takumi Yoshida (The University of Tokyo) for the help of various measurements.

I am strongly grateful to Prof. Dr. Tohru Fukuyama, Prof. Dr. Satoshi Yokoshima, and assistant Prof. Dr. Yoshitake Nishiyama for giving me fundamental of research skills.

I am deeply thankful to SHOSHISHA foundation for the financial support to encourage my research.

Finally, I would like to express sincerely appreciation for my family, Mr. Shunji Yonezawa, Mrs. Keiko Yonezawa, Mr. Yutaka Yonezawa, Mrs. Midori Yonezawa, Satoshi Hiraiso, Mrs. Motoe Hiraiso, Mr. Masanori Yonezawa, Mr. Kazuyuki Yonezawa for their special supports to date.

米澤拓孝

Hirotaka Yonezawa